Chemical Geology 616 (2023) 121215

Contents lists available at ScienceDirect

Chemical Geology

journal homepage: www.elsevier.com/locate/chemgeo

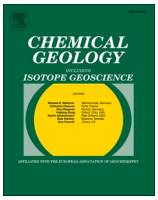

Can element chemical impurities in aragonitic shells of marine bivalves serve as proxies for environmental variability?

Bernd R. Schöne [a,*], Soraya Marali [a], Anne Jantschke [a], Regina Mertz-Kraus [a], Paul G. Butler [b], Lukas Fröhlich [a]

[a] Institute of Geosciences, University of Mainz, Johann-Joachim-Becher-Weg 21, 55128 Mainz, Germany
[b] Centre for Geography and Environmental Sciences, College of Life and Environmental Sciences, University of Exeter, Treliever Road, Penryn, Cornwall TR10 9FE, UK

ARTICLE INFO

Editor: Michael E. Boettcher

Keywords:
Bivalve sclerochronology
Shell
Element chemistry
Environmental proxy
Reproducibility

ABSTRACT

In many biogenic and geogenic materials, ion impurities can provide serviceable proxies for environmental conditions. However, the element/Ca ratios of bivalve shells are notoriously challenging to interpret. Due to strong vital effects, nonclassical nucleation and growth mechanisms, and/or kinetic processes, the concentration of trace and minor elements in marine shells typically remains below values observed in inorganic $CaCO_3$ precipitated from a solution resembling seawater chemistry but above those expected for thermodynamic equilibrium. The interpretation is further complicated by non-lattice bound and microstructure-specific element content. If environmental conditions were still encoded in the shells, they should result in statistically significantly reproducible element/Ca chronologies between contemporaneous specimens from the same site. Here, we tested this hypothesis and exemplarily studied seven elements in twelve modern specimens of *Arctica islandica* collected from four different localities in the North Atlantic (Faroe Islands, NE Iceland, Isle of Man, Gulf of Maine). Age-detrended chronologies of weighted annual B, Mg, Sr and Ba/Ca ratios (Al, Zn and Pb largely remained below detection limit) measured in the shells were reproducible between most specimens from the same site, supporting the hypothesis that the incorporation of these elements was at least partly controlled by environmental forcings. Notably, the agreement (explored with linear regression analyses and sign tests) between shell element/Ca ratios and environmental quantities was weaker than the agreement of respective element/Ca ratios between specimens suggesting that the available information on temperature, food and water chemistry did not properly reflect the in-situ conditions to which the bivalves were exposed or other extrinsic factors were at work. As in inorganic aragonite – but in contrast to thermodynamic expectations –, annual Sr/Ca, Mg/Ca and B/Ca ratios were negatively correlated to water temperature (up to 40% explained variability). The link between Ba/Ca and bulk phytoplankton often remained below the significance threshold, but was otherwise positive. Quantitative environmental reconstructions based on ion impurities in bivalve shells will remain challenging or impossible unless the chemistry of the parent solution (= extrapallial fluid) from which the shell actually formed is known, including temporal changes thereof. This information is crucial to compute representative partition coefficients required to calibrate transfer functions.

1. Introduction

Shells of bivalves have emerged as a powerful and widely used paleoenvironmental archive. This success is partly based on periodic changes of their biomineralization rate which leave distinct time markers in the shell (Barker, 1964) in the form of circatidal, daily, fortnightly and annual growth lines (= periods of slow growth) and increments (= main growing season) (e.g., Evans, 1972; Clark II, 1974; Jones, 1980). Growth patterns provide a means to determine the ontogenetic age of bivalves and place the shell proxy data into an accurate temporal context. Long-lived species such as *Arctica islandica* (up to 500 years; Schöne et al., 2005; Wanamaker Jr et al., 2008; Butler et al., 2013) have received particular attention, because their shells not only inform about seasonal to inter-annual changes of biological and/or environmental variables, but also reveal trends and lower-frequency oscillations in the climate system (e.g., Schöne et al., 2003; Black et al., 2009; Butler

* Corresponding author.
E-mail address: bernd.schoene@uni-mainz.de (B.R. Schöne).

https://doi.org/10.1016/j.chemgeo.2022.121215
Received 21 June 2022; Received in revised form 9 November 2022; Accepted 10 November 2022
Available online 15 November 2022

et al., 2010; Wanamaker Jr et al., 2012, 2019; Lohmann and Schöne, 2013; Reynolds et al., 2016, 2017; Edge et al., 2021). Such reconstructions can cover time intervals of >1000 years (Wanamaker Jr et al., 2012; Butler et al., 2013; Holland et al., 2014a) if increment width series of specimens with overlapping lifespan are combined to form longer, replicated chronologies by means of crossdating (Jones et al., 1989; Weidman et al., 1994; Witbaard et al., 1997; Marchitto Jr. et al., 2000).

Despite many outstanding bivalve sclerochronological discoveries, however, the number of reliable and well-accepted environmental proxies remains limited. Specifically, the potential use of trace and minor elements in shells as surrogates for environmental variables is controversially debated (Peharda et al., 2021). Due to strong biological controls on the incorporation of many elements into shells (i.e., vital effects), non-classical nucleation processes (De Yoreo et al., 2015; Boon et al., 2020; Gilbert et al., 2022) etc., their concentration often deviates from values observed in inorganic $CaCO_3$ as well as thermodynamic predictions and varies with the prevailing shell microstructure and shell organics (Schöne et al., 2010, 2013; Izumida et al., 2011; Shirai et al., 2014; Yoshimura et al., 2014; Roger et al., 2017). For example, Sr/Ca values in shells of *A. islandica* (Schöne et al., 2011, 2013; Wanamaker and Gillikin, 2019; Brosset et al., 2022) can attain 3 to 4 mmol/mol at annual growth lines (often consisting of irregular prismatic / spherulitic microstructure), but only ca. 0.5 to 1 mmol/mol in annual growth increments (e.g., homogenous and crossed microstructures), which is approx. 3 to 24 times lower (assuming temperature = 2–15 °C, Sr/Ca_{water} = 8.67 mmol/mol cf. https://www.mbari.org ["Periodic Table of Elements in the Ocean", last access: 16 May 2022], hereafter referred to as 'MBARI') than Sr/Ca ratios of inorganic aragonite (e.g., Gaetani and Cohen, 2006). In species in which Sr/Ca_{shell} ratios and water temperature are – as expected from synthetic aragonite – negatively correlated, the temperature sensitivity of Sr/Ca_{shell} often deviates from that of inorganic aragonite (Yan et al., 2013, 2014; Füllenbach et al., 2015; Zhao et al., 2017a) providing another line of evidence that the incorporation of trace and minor elements into bivalve shells is subject to vital effects.

The calibration and application of element-based environmental proxies is further complicated by the fact that cations may not only substitute for Ca^{2+} in the crystal lattice of $CaCO_3$, but can also be covalently bound to organic matrices of the shell (Foster et al., 2008; Takesue et al., 2008; Schöne et al., 2010; Izumida et al., 2011; Yoshimura et al., 2014), occur as inorganic nanoparticles (Foster et al., 2008; Fritz et al., 1990; Yoshimura et al., 2014) or can be adhesively adsorbed onto crystal surfaces (Izumida et al., 2011). The composition of the shell organics is relevant as well. For example, Mg^{2+} is typically associated with phosphorous- and sulfur-bearing organics (Roger et al., 2017), but Sr^{2+} with sulfur-rich organics (Shirai et al., 2014). Unfortunately, it is currently impossible to determine the chemistry of the different organic compounds of the shell. In particular, the chemical composition of the water-soluble intra-crystalline organics cannot be determined, because it seems nearly impossible to isolate this phase from the insoluble organics as well as the mineral or – if present – amorphous phases.

However, not just the fate but also the sources of elements in bivalve mollusk shells are far from being entirely understood: Are shell impurities deriving entirely from free (hydrated), hydrolyzed or complexed ions in the water (for a compilation of inorganic species of dissolved elements in seawater see Bruland, 1983 and Byrne, 2002) or do they also originate from elements bound to particles and colloids? In the case of barium, background levels in the shell are likely sensitive to changes of dissolved Ba in water (Komagoe et al., 2018) and salinity (Gillikin et al., 2008; Poulain et al., 2015). Sharp erratic Ba/Ca_{shell} peaks, however, appear to be linked to specific diatoms and dinoflagellates (Thébault et al., 2009; Fröhlich et al., 2022a) rather than bulk phytoplankton (Stecher III et al., 1996; Vander Putten et al., 2000; Lazareth et al., 2003). The same applies to Li and Mo/Ca_{shell} (Thébault et al., 2022; Fröhlich et al., 2022b).

Furthermore, a sudden chemical change in the ambient water may not become immediately encoded in the shell. Some elements, specifically heavy metals, can be stored in insoluble, organic-coated extracellular granules (Thomson et al., 1985) or bound to specific proteins (Viarengo, 1989; Roesijadi, 1992) for several months, years or even the entire lifetime of the animal. Respective elements may thus only arrive in the shell with a considerable time lag or not at all (Schöne and Krause, 2016).

Considering the uncertainties of element uptake from the environment, transport and storage within the body, and incorporation into the shell, it would not be appropriate to evaluate the potential use of shell element chemical properties as environmental proxies primarily or exclusively by comparison with environmental data. A more useful approach is to assess the chemical reproducibility between contemporaneous specimens from the same habitat (e.g., Stecher III et al., 1996; Gillikin et al., 2008). Marali et al. (2017a) accomplished this with annual shell Na, Mg, Mn, Sr and Ba/Ca time-series of six modern *A. islandica* specimens from two localities (three each from the Gulf of Maine and the Isle of Man). Element/Ca series of contemporaneous specimens varied synchronously, in particular Ba/Ca_{shell}, but also Sr and Mg/Ca_{shell} (Marali et al., 2017a; see also Marali et al., 2017b), suggesting external forcings. Ontogenetic age, growth rate and microstructure were identified as additional contributors to element chemical data, but their influence was not adjusted for.

The present study builds on the findings of Marali et al. (2017a). We have re-investigated and reprocessed their data (in particular for reproducible element series, i.e., Mg, Sr and Ba/Ca_{shell}), included six more specimens from two more localities (NE Iceland, Faroe Islands), and assessed four additional element/Ca ratios (B, Al, Zn, and Pb/Ca_{shell}). More sophisticated mathematical techniques were applied to identify if these elements were controlled by external forcings and might therefore provide potential for paleoenvironmental reconstructions. Specifically, we have applied a more advanced signal extraction method considering the circular geometry of the sample spots, and computed weighted annual averages to account for seasonally varying growth rates and thus time-averaging (Schöne et al., 2022). Prior to comparison of the chronologies, ontogenetic age and/or growth rate-related trends were mathematically eliminated from the data. We also took potential temporal alignment errors of one year as well as outliers into consideration, i.e., individual specimens that showed chemical patterns different from other specimens. In addition to linear regression analyses, sign tests were employed to evaluate the strength of the relationship among element chemical chronologies from the same locality as well as shell chemistry and environmental variables. The methodological approach used here may serve as a guideline for subsequent element chemical studies of mollusk shells. Results of this study indicate which elements of bivalve shells can potentially serve as environmental surrogates.

2. Material and methods

2.1. Sample material, preparation and growth pattern analysis

Twelve specimens of *A. islandica* were obtained by dredging from NE Iceland (ICE, water depth = 9–11 m, N = 4), the Isle of Man (IOM, 30–57 m, N = 3) and the Gulf of Maine (GOM, 83 m, N = 3) (Table 1; see map in Marali et al., 2017b). Specimens from the Faroe Islands (FO, 20 m, N = 2) were obtained by SCUBA diving within a fjord between the islands of Streymoy and Vágar (SE of the city of Vestmanna). This locality is potentially more strongly influenced by freshwater runoff from land than the other study sites. The long-term average temperature equals 9 °C. Specimens from ICE came from Þistilfjörður, a large bay west of Langanes pensinusla, SW Þórshöfn. Although a small river flows into the bay, salinity in close to 34.8. Average temperatures are ca. 4 °C. The area lies near Polar Front and is variably affected by the warm Irminger Current and cold East Iceland Current. Specimens from IOM

Table 1
List of *Arctica islandica* shells used in present study. Except for specimen IOM0525475R, all bivalves were collected alive. WD = water depth; Age = ontogenetic age.

Specimen ID	Locality	WD (m)	Latitude/Longitude (WSG84)	Age (yr)	Coverage (yr CE)
FO10–10-01-V6AR1	Faroe Islands	20	62°09′15.00”N, 007°10′25.00”W	114	1895–2006
FO10–10-02-V12AR1				155	1855–2005
IOM0525475R	Isle of Man	40	54°07′15.00”N, 004°52′20.40”W	250	1758–2002
IOM0505327R		30	54°18′34.80”N, 004°43′14.40”W	87	1919–2003
IOM0505319L		57	54°08′25.80”N, 004°53′58.80”W	82	1923–2002
ICE120501AL1	NE Iceland	9	66°09′58.92”N, 015°22′58.92”W	70	1946–2010
ICE121401AL1		10	66°11′28.98”N, 015°20′25.44”W	176	1839–2007
ICE120703AL2		11	66°11′13.68”N, 015°20′48.30”W	178	1837–2006
ICE120505AL2		9	66°09′58.92”N, 015°22′58.92”W	80	1936–2008
GOM090797R2	Gulf of Maine	83	44°26′09.83”N, 067°26′18.05”W	47	1963–2008
GOM090803R3				57	1953–2007
GOM090829R1				60	1953–2008

potentially experienced stronger pollution because the sample area is surrounded by more densely populated regions than the other studied sites. Average temperature and salinity are 10 °C and 34.2, respectively. GOM bivalves were collected ca. 20 km away from the coast in water that attain, on average, 6.5 °C and 32.2 PSU.

As revealed by crossdating (Butler et al., 2010; Marali et al., 2017b), one bivalve from the IOM died two years prior to collection, all others were captured alive and soft parts removed soon afterward. For a detailed description of the shell preparation, growth pattern analysis and crossdating see Marali et al. (2017a). Briefly, two approx. 3 mm-thick sections were cut from each shell, ground on glass plates (F800/1200 grit SiC powder suspended in water) and polished on Buehler G-cloth (with 1 μm Al_2O_3 powder suspended in water). Annual increment width analyses were completed in the hinge portions of the shells using Mutvei-stained sections (ICE + FO: Marali et al., 2017b) or peel replicas (IOM: Butler et al., 2010; GOM: Griffin, 2012). Growth patterns analysis was used to place the shell record into temporal context.

2.2. In-situ chemical analysis (LA-ICP-MS)

The remaining polished hinge portions were used for in-situ chemical analysis at the Institute of Geosciences at the University of Mainz by means of a Laser Ablation - Inductively Coupled Plasma - Mass Spectrometry (LA-ICP-MS) system consisting of a 193 nm ArF Excimer laser (ESI NWR193) coupled to an Agilent 7500ce quadrupole ICP-MS. Prior to the measurements, pre-ablation was used to clean the sample surface and remove potential contaminants from the upper approx. 0.6 μm. To do so, a LA spot size of 100 μm was applied in line scan mode with 3 Hz, 50 μm/s scan speed at an energy density of about 3 J/cm^2. Then, measurements were done in line scan mode (scan speed = 5 μm/s; beam diameter = 55 μm; laser repetition rate = 10 Hz; laser energy on samples ~7 J/cm^2; sample depth approx. 15 μm). The distance between laser spot positions at which a new data acquisition cycle started equaled approx. 1.45 μm. Prior to each line scan, background intensities were measured for 20 s.

Accuracy and precision of the analyses were monitored with NIST SRM 610, USGS BCR-2G and USGS MACS-3 measured before and after each line scan. With these data, we have computed element-specific RSD % (RSD = relative standard deviation) values and average limits of detection (LOD; $3\sigma_{background}$ according to Jochum et al., 2012). NIST SRM 612 was used to calibrate the element concentrations of shells and other reference materials using preferred values reported in the GeoReM database (available at http://georem.mpch-mainz.gwdg.de, ver. 30, last access: 1 Mar 2022; Jochum et al., 2005, 2011). Concentrations of the following elements were determined: boron (measured as intensity of ^{11}B), magnesium (^{25}Mg), aluminum (^{27}Al), zinc (^{66}Zn), strontium (^{88}Sr), barium (^{137}Ba) and lead (^{208}Pb). ^{43}Ca served as internal standard for reference materials and shells. Calcium concentrations for the reference materials were taken from the GeoReM database, and for the shells we used a value of 380,000 μg/g following Marali et al. (2017a). For a full set of data including sodium (^{23}Na), potassium (^{39}K) and manganese (^{55}Mn) vs Ca data as well as calculations see Supplements in Schöne et al. (2022) and data summary in Supplements 1 of present paper. Note, shell B, Mg, Al and Sr/Ca ratios are reported in mmol/mol, and Zn, Ba and Pb/Ca in μmol/mol.

2.3. Data processing

LA-ICP-MS data obtained in line scan mode come with much higher scatter than results from single spot analysis along the same transect would reveal. To extract signals from such noisy data, we have applied the 38-pt circle segment area-based weighted moving average filtering method described by Schöne et al. (2022). This approach accounted for the distance the laser traveled between successive data acquisitions cycles as well as for the geometry of the laser spots on the sample surface. With this discretization method, the continuous line scan data with overlapping sampling spots were converted into a new chronology with non-overlapping data (see also Fox et al., 2017).

Subsequently, the new, discretized data were placed in temporal context, i.e., the centers of the data points were dated to the nearest day by using water-depth specific seasonal growth models for *A. islandica* (Höche et al., 2022). Gaps between the temporally aligned data were filled by linear imputation in order to obtain daily element/Ca_{shell} chronologies. With these data it was possible to compute weighted annual averages (see Schöne et al., 2022, for more details).

Directed ontogenetic trends toward higher or lower values were mathematically eliminated (Supplements 1). For this purpose, annual element/Ca_{shell} data were plotted against ontogenetic age and stiff cubic splines or suitable (exponential, linear) equations fitted to the data to estimate the long-term trends. Instead of producing dimensionless element/Ca_{shell} data, the lowest value was set as an anchor point, and other element/Ca_{shell} values decreased by the difference (offset) between this anchor point and the predicted element/Ca_{shell} ratio at the respective stage of life.

Alternative to ontogenetic age trends, the correlation with shell growth rate was removed from the element chemical data. Similar to the method described above, annual element/Ca_{shell} data were plotted against increment width and cubic splines, natural logarithms or power functions fitted to the data. Then, the anchor point method was used to hinge the element/Ca_{shell} data at the smallest value and decrease other element chemical data by the offset between the anchor point and the predicted value at the respective increment width. Furthermore, a

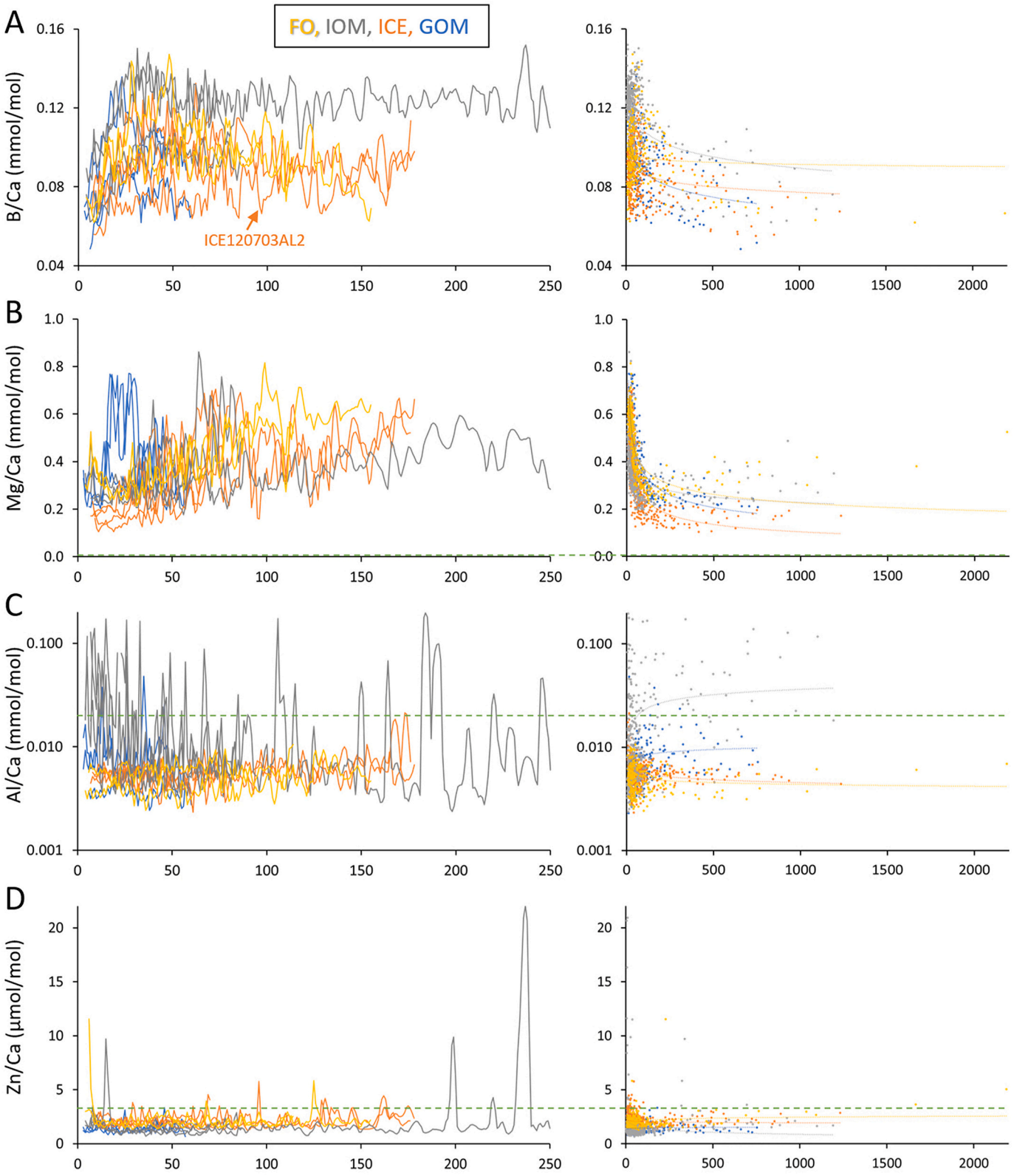

Fig. 1. Shell element/Ca data of *Arctica islandica* (hinge portion) plotted against ontogenetic age (left panels) and annual increment width (right panels). All studied element/Ca series showed directed trends toward higher or lower values through lifetime. B, Mg and Sr/Ca also revealed distinct non-linear relationships with shell growth rate. Except for Mg/Ca and Sr/Ca (power functions), logarithmic equations provided the best fit. Detection limits are indicated by green dashed line (not provided for elements were LOD is far below scale of y-axis). FO = Faroe Islands, IOM = Isle of Man, ICE = NE Iceland, GOM = Gulf of Maine. To inspect individual chronologies in more detail and assess shell Na, K and Mn/Ca data, the reader is referred to Supplements 1 + 3. (For interpretation of the references to colour in this figure legend, the reader is referred to the web version of this article.)

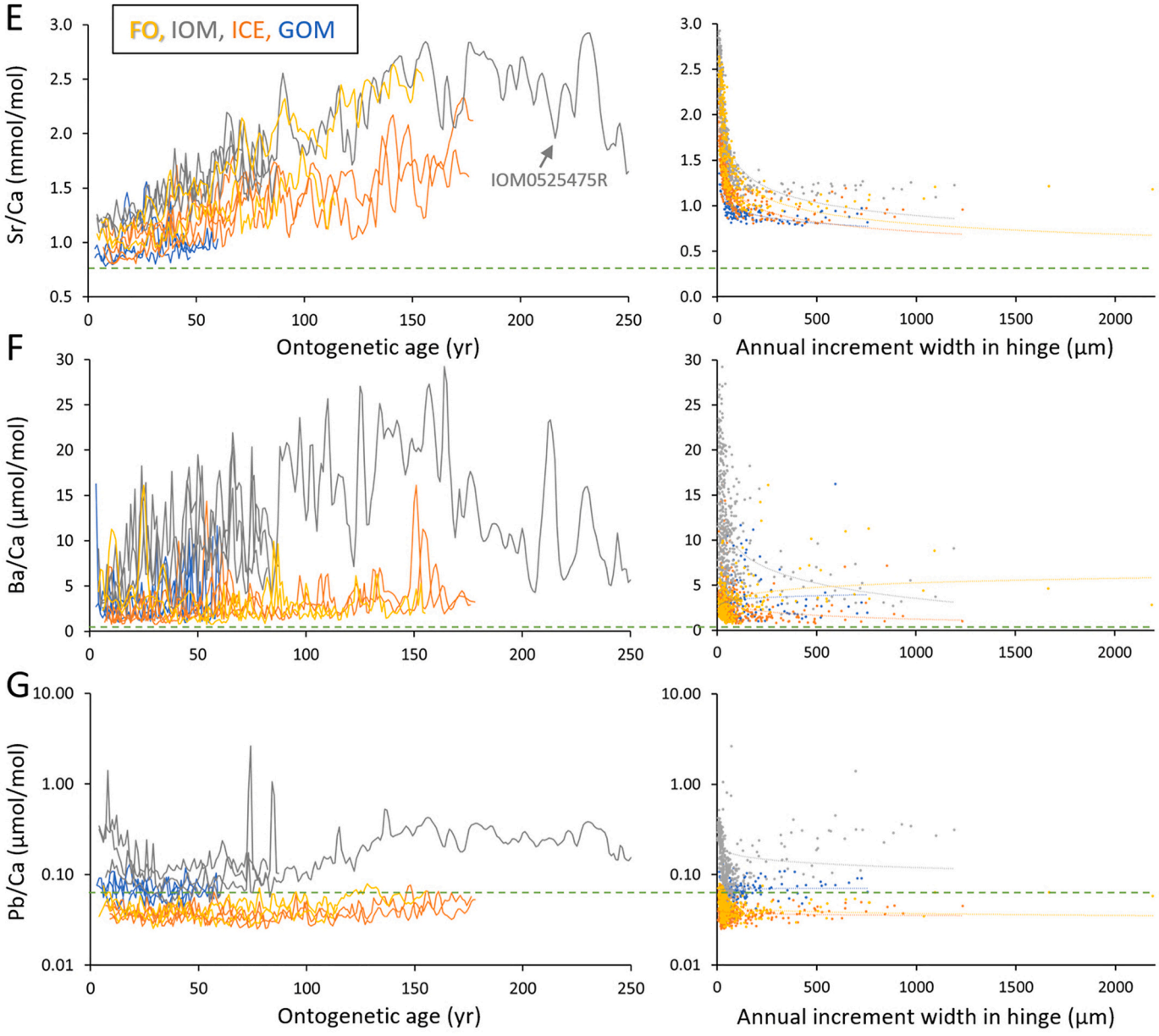

Fig. 1. (*continued*).

double detrending was explored, i.e., after removal of ontogenetic age-related trends, the correlation of the residuals with growth rate was mathematically eliminated.

2.4. Statistical analysis

Mathematical relationships between detrended element chemical properties were quantified by linear regression analysis (Pearson correlation) and sign tests (running dis/similarity analyses; Eckstein and Bauch, 1969; similarity: G values expressed in %; dissimilarity: D values expressed in %; for calculation template see Supplements 2). Significant running similarity (aka 'Gleichläufigkeit') exists if the inter-annual changes of two chronologies are highly congruent, i.e., the direction of change between years is identical in a significant number of instances (i.e., signs are similar). Significant running dissimilarity (aka 'Gegenläufigkeit') indicates that a significant number of inter-annual changes of the two chronologies move in opposite directions (i.e., signs are different).

To account for individual differences, chronologies of the same site were not only compared on an individual basis ('one-by-one comparison'), but each chronology (one at a time) was also compared to the average of the remaining chronologies from the same locality ('one-versus-others comparison'), an approach similar to that traditionally employed in dendrochronology for crossdating purposes (software COFECHA: Holmes, 1983). In the main text, only the highest correlations or G values of each element/Ca_{shell} value are reported and discussed; for a more detailed overview of the results, the reader is referred to the Supplements (part 3). Note, the one-versus-others approach is superior to the comparison of two individual time-series, because the latter requires that both chronologies are perfectly temporally aligned, whereas the former is more resilient against alignment errors. In the one-versus-others approach, potential errors in annual growth increment identification are evened out by the calculation of an average chronology. To further account for missing or falsely identified annual growth increments and subsequent errors in temporal alignment as well as to take temporal lags in response to environmental changes into

consideration, the chronologies were smoothed (= low-pass filtered) with a weighted moving average (filter weights: $t_0 = 100$, t_1 and $t_{-1} = 68$, t_2 and $t_{-2} = 32$).

Aside from assessing the relationship between specimens, the agreement between locality-specific element chronologies ([i] arithmetic average of all studied chronologies; [ii] arithmetic average of all but one chronology) and environmental chronologies was evaluated (for source of environmental data sets see Supplements 1). With respect to the latter, the focus was placed on element/Ca_{shell} data for which a causal link has repeatedly been described before in bivalves, i.e., Sr/Ca and Mg/Ca vs water temperature (T) (Dodd, 1965; Schöne et al., 2011; Yan et al., 2014), as well as Ba/Ca vs chlorophyll *a* concentration (Chl a) (e.g., Stecher III et al., 1996; Vander Putten et al., 2000; Lazareth et al., 2003). Exploratively, the link between B/Ca and T (McCoy et al., 2011) as well as Ba/Ca vs T was investigated (e.g., Wanamaker and Gillikin, 2019). As before, raw and digitally filtered chronologies including a lead or lag of one year were computed, and only the highest correlation coefficients, coefficients of determination, and dis/similarity values are reported in the main text (full data set in Supplements 3).

3. Results

3.1. Ontogenetic shifts of shell element chemical properties

Almost all element/Ca_{shell} chronologies revealed ontogenetic trends – though different in magnitude – toward (overall) higher (B, Mg, Sr, and Ba/Ca) or lower values (Pb/Ca) (Fig. 1; see Supplements 1 for details as well as Na, K and Mn/Ca data). Due to decadal variability, the trends were typically easier to identify in the long chronologies of IOM, ICE and FO than the shorter (47 to 60 yr-long) series of GOM (Fig. 1; Table 1). As the great majority of Al/Ca and Zn/Ca data remained below detection limit (0.02 mmol/mol and 3.27 μmol/mol, respectively), no assessment of trends can be provided for these elements.

The slopes of the trends varied considerably between elements and sites, and sometimes even among contemporaneous specimens from the same locality (Fig. 1). For example, B/Ca increased sharply in almost all studied specimens during the first three to four decades of life (except for specimen ICE120703AL2 which showed a relatively steady increase through ontogeny from 0.07 to 0.09 mmol/mol), reached a maximum and then fluctuated around a steady level or gently declined (Fig. 1A). With approx. 0.12 mmol/mol, the average plateau value was approx. 0.03 mmol/mol higher in specimens from IOM than in shells from the other three sites (Fig. 1A). At IOM and GOM, B/Ca values differed, on average, by the same amount between specimens (Fig. 1A).

In other elements with overall positive trends, the increase often started only after an early ontogenetic decrease and ended with the attainment of an element- and specimen-specific plateau value, typically after the age of ca. 150 years or so (Fig. 1). Instead of fluctuating around a constant level, the concentration of some elements declined after the maximum was reached. For example, Mg/Ca values typically declined exponentially during the first two decades of life by approx. 20 to 40%, reached a minimum at around age 20 and then rose nearly linearly up until age 200 (specimen IOM0525475R). Thereafter, the slope rapidly leveled-off and eventually the sign became negative, i.e., Mg/Ca values declined again. The average Mg/Ca level at age 250 was about the same as what it had been at age 130 (approx. 0.35 mmol/mol) (Fig. 1B). The ontogenetic Mg/Ca trends of two young specimens from GOM differed from the above-mentioned pattern. In GOM090829R1 and GOM090803R3, Mg/Ca sharply increased by >100% between age 12 and 18, stayed at that level for about 20 years and then dropped again (Fig. 1B).

The average decline of Sr/Ca during early ontogeny was smaller (ca. 10 to 20%) than of Mg/Ca, but values likewise increased steadily and nearly linearly afterward (on average, from around 1.0 mmol/mol at age 20 to 2.2 mmol/mol at age 170) (Fig. 1E). In the oldest specimen (IOM0525475R), highest Sr/Ca levels were attained at around age 170, followed by a gentle decline toward the end of life (age 250: 1.8 mmol/mol as at age 70) (Fig. 1E). Regression slopes varied notably between localities and were shallowest at GOM and ICE and steepest at IOM and FO (Fig. 1E). Accordingly, specimens from the latter two localities reached higher Sr/Ca values (ca. 2.5 mmol/mol) than those at ICE at the age of 170 (1.6 mmol/mol) (Fig. 1E). As in Mg/Ca, the slope of Sr/Ca chronologies occasionally varied considerably between specimens from the same site. The strongest difference was observed at FO. In specimen FO10–10-01-V6AR1, Sr/Ca_{shell} increased by 0.005 mmol/mol per year, whereas the increase was twice as strong in specimen FO10–10-01-V12AR1 (Fig. 1E).

Similar to Sr/Ca, after a gradual increase, Ba/Ca values reached a plateau at about age 130 and started to decline after age 160 (IOM0525475). When the oldest studied specimen died (age 250), the average Ba/Ca values had fallen back to about the same level as at age 40 (approx. 6 μmol/mol) (Fig. 1F). The slowest relative increase was observed in Sr (30% in 100 years), followed by Ba (approx. 50%), and the sharpest rise was in Mg/Ca (doubling in 100 years) (Fig. 1).

Among the elements that revealed overall ontogenetic trends toward lower values (Pb: Fig. 1G; Na, Mn: Supplements 1), only Na/Ca decreased monotonously through lifetime (Supplements 1). Pb/Ca in specimens from IOM attained lowest levels at the age of ca. 70 years and then rose. In the oldest studied specimen (IOM0525475R), at the age of ca. 160, Pb returned to values obtained from shell portions formed during youth. Thereafter, a gentle decline was observed (Fig. 1G). Pb/Ca remained below LOD (0.07 μmol/mol) at ICE and FO, but still showed trends similar to those at IOM (Fig. 1G). At GOM, Pb/Ca occasionally exceeded the LOD and gently declined through ontogeny. In Na and Pb/Ca, the ontogenetic decrease was typically exponential, and the subsequent rise in Pb/Ca non-linear (Fig. 1G; Supplements 1).

All chronologies of studied elements exceeding the LOD showed oscillations on quasi-decadal and shorter time-scales (Fig. 1), most distinctly developed in Mg/Ca and Sr/Ca (Fig. 1B, E). While the interannual variability decreased during lifetime, the lower frequency (= decadal) oscillations became stronger with increasing age, i.e., their amplitudes increased (Fig. 1; Supplements 1). This was particularly well seen in B, Na, Mg and Sr/Ca, but also in Ba and Pb/Ca (Fig. 1A, B, E–G; Supplements 1). Aside from decadal variations, some element chronologies (Al, Zn, Ba, and Pb/Ca) were interrupted by sharp peaks which exceeded background levels by multiple times (Fig. 1C, D, F, G). For example, Al/Ca peaks were up to 5800% larger than background levels (and were clearly above the LOD) (Fig. 1C). In Zn/Ca, peaks exceeded the background values by up to 2400% (likewise above LOD) and were less frequent than in Al/Ca (Fig. 1C, D).

3.2. Growth rate-related changes of shell element chemical properties

Besides being linked to ontogenetic age, five of the studied element/Ca values were also non-linearly coupled with shell growth rate, positively in case of Na and Mn (Supplements 1), and negatively in case of B/Ca, Mg/Ca and Sr/Ca_{shell} (Fig. 1A, B, E). Natural logarithms typically provided the best fit to describe this relationship, but for Mg/Ca and Sr/Ca, power functions were often more useful, because the slope of the relationship changed very rapidly (Fig. 1B, E). Among all shell element/Ca ratios, Sr/Ca showed the strongest link to increment width (Fig. 1E). R^2 values ranged between 0.48 and 0.73 for logarithmic fits, and 0.51 to 0.76 when power functions were used (the latter are depicted in Fig. 1E). Mg/Ca and Sr/Ca dropped sharply as increment width increased from approx. 10 to 100 μm, i.e., on average, 0.70 to 0.30 and 2.50 to 1.20 mmol/mol, respectively (Fig. 1B, E). The regression curves gradually shallowed as growth rate further increased (Fig. 1B, E). Above an increment width of 250 μm, both element-to-Ca ratios were slightly positively correlated with growth rate, i.e., above this threshold, faster growing hinge portions contained increasingly higher amounts of Mg and Sr relative to Ca (Fig. 1B, E). In both elements, the change from a negative to a positive relationship were neither well captured with

power functions nor natural logarithms (Fig. 1B, E). In B/Ca, the regression slope likewise leveled-off with increasing growth rate, but no change in the sign of the slope was observed (Fig. 1A). With 0.01 to 0.33, R^2 values remained well below those of Mg/Ca (0.26 to 0.60, ln-fits). In contrast to Mg, Sr and B, Na/Ca strongly increased with growth rate up to an increment width of about 100 μm (from approx. 18 mmol/mol at 10 μm to 21 mmol/mol at 100 μm), thereafter the regression curve gradually shallowed (Supplements 1). The same was observed for Mn/Ca at GOM and IOM, but the slope of the relationship decreased more gradually than in Na/Ca (Supplements 1). At the other two localities, Mn content remained below LOD prohibiting a meaningful assessment (Supplements 1). In the remaining four studied elements (Al, Zn, Ba and Pb), the relationship with increment width was either very weak or impossible to assess because data remained below LOD (Fig. 1C, D, F, G). In slow-growing shell portions, Ba and Pb showed larger variability than in faster growing shell portions (Fig. 1F, G).

3.3. Relationship between detrended element chronologies of contemporaneous specimens from the same locality

Averaged over the studied elements, specimens from GOM showed the strongest agreement (positive linear correlation and running similarity) between corresponding chronologies (maximum age difference between specimens: 13 years), closely followed by specimens from ICE (108 years difference) and IOM (168 years difference) (Fig. 2; Table 2). The weakest relationship occurred among the two specimens from FO (41 years difference). At GOM, the average r value of the seven studied elements – computed from the strongest (though not always statistically significant; see further below) positive linear correlations between two specimens (= one-by-one comparison) – was 0.68, while respective r values for ICE, IOM and FO equaled 0.66, 0.47 and 0.09, respectively (Fig. 2A; Table 2; Supplements 3). If the strongest correlation between the element chronology of one specimen versus the average chronology of all other specimens of the same locality was considered (= one-versus-others comparison; not possible to provide for FO), the average r values remained nearly unchanged (GOM: 0.67; ICE: 0.64; IOM: 0.43) (Fig. 2B; Table 2). Sign tests reflected these differences (Fig. 2A, B; Table 2), i.e., G values were 67 (GOM), 65 (ICE), 64 (IOM) and 53% (FO) for one-by-one comparisons, and 71 (GOM), 62 (ICE) and 63% (IOM) for one-vs-others comparisons, respectively. Except for FO, r values were higher when high-frequency components were eliminated (one-by-one: 0.74, 0.68, 0.56, and 0.05 for GOM, ICE, IOM and FO, respectively; one-versus-others: 0.72, 0.61, 0.49 for GOM, ICE and IOM, respectively), but running similarity remained largely unchanged (Fig. 2C, D; Table 2).

Correlation and running similarity between chemical data of contemporaneous specimens not only varied between sites but also among the different elements (Fig. 2; Table 2). In general, statistically significant correlation occurred more frequently between the studied element chronologies than significant running similarity (Fig. 2; Table 2). In a few cases (Sr at FO and Pb at IOM and GOM), significant running similarity was identified, while correlation remained insignificant (Fig. 2; Table 2). At all localities except FO, B, Mg and Sr/Ca chronologies of contemporaneous specimens from the same site were consistently highly significantly ($p < 0.05$) correlated with each other (Fig. 2; Table 2). With some exceptions this result was reflected by significant running similarity (Fig. 2; Table 2). B/Ca reached r values of up to 0.92 (GOM), Mg/Ca 0.88 (GOM) and Sr/Ca 0.90 (ICE). G values for these elements were as high as 82 (GOM), 79 (ICE), 79 (GOM) and 77% (ICE). Of all studied elements, Ba/Ca chronologies showed the strongest linear correlation and running similarity among contemporaneous specimens from the same locality (r values of up to 0.96 and G values of up to 88%), but only at IOM, ICE and GOM (Fig. 2; Table 2). At FO, Ba/Ca series were not in synchrony. In almost all instances, Na/Ca chronologies of co-occurring specimens from the same site were moderately to strongly linked to each other (r values of up to 0.81), but running similarity was only significant at ICE and GOM (G values of up to 69%) (Supplements 1). Weak positive links were found among Pb/Ca chronologies at GOM and IOM (Fig. 2; Table 2). As before, no meaningful assessment was possible of elements remaining largely below LOD, i.e., Al/Ca and Zn/Ca at all sites as well as Pb/Ca at FO and ICE (Fig. 2; Table 2).

3.4. Relationship between detrended element chronologies and environmental properties

Water temperature and age-detrended Sr/Ca ratios were statistically significantly correlated at all sites, although the relationship was positive at GOM and only weakly negative at FO (Fig. 3; Table 3). The strongest negative correlation was observed at ICE. At this locality, up to 30% of the year-to-year variability in Sr content of the shell was explained by changes in water temperature (25% if an alignment error of −1 year was taken in account) (Fig. 3D; Table 3). This finding was corroborated by a strong visual agreement between the temperature curve and the ontogenetic age-detrended Sr/Ca series (for both the individual chronologies as well as the average chronology), specifically on decadal and multidecadal time-scales (Fig. 4). Furthermore, the running dissimilarity (Sr, Mg, Ba and B/Ca chronologies are expected to run counter to temperature curves) between Sr/Ca and temperatures was statistically significant at ICE and IOM, but not at the other two localities, even after low-pass filtering was applied (Fig. 3; Table 3).

Age-detrended Mg/Ca series showed the strongest (consistently negative) correlation with temperature at IOM (17% explained variability, 21% when filtered, and 32% when an alignment error of −1 year was considered and data of one specimen were omitted from the analysis) (Fig. 3; Table 3). Running dissimilarity exceeded the significance level if one chronology (showing the weakest agreement with the others) was omitted (FO, IOM) and the data were low-pass filtered (D values at all localities below $p < 0.05$) (Fig. 3; Table 3). Growth rate-detrended Ba/Ca correlated strongly with Chl a at FO, ICE and GOM, and mostly showed significant running similarity unless non-filtered series of individual specimens were compared with each other (Fig. 3C, D; Table 3). Note that available Chl a chronologies at FO, ICE and GOM comprised only a few years (8 to 10; due to end-fitting problems 4 years less after low-pass filtering) limiting the explanatory power of the r values. Growth rate-detrended shell Ba/Ca was only significantly correlated with water temperature at FO and IOM (up to 21% explained variability), but D values remained below significance level. The strength of agreement improved after digital smoothing (up to 32% explained variability and 65% running dissimilarity at IOM) (Fig. 3; Table 3).

In addition to the detrending methods described in Section 2.3, alternative approaches were exemplarily tested for shell Sr/Ca data from ICE (Supplements 4): (i) Growth rate-detrending of the element chemical data resulted in lower agreement with environmental data sets than age-detrending. (ii) A double-detrending, i.e., growth rate-detrending of age-detrended data, increased the correlations only marginally compared to data corrected only for age relationships (R^2 values were increased by merely 0.01 or so). After age-detrending, the residuals did not reveal any distinct or significant relationship with increment width any more. If data pairs from early ontogeny were discarded, i.e., only element data from slow-growing portions (growth increments <100 μm) were considered, many elements were strongly non-linearly correlated with growth rate. However, the use of such data in the double detrending approach did not improve correlation, neither between Sr/Ca chronologies of contemporaneous specimens, nor between Sr/Ca time-series and environmental variables (Supplements 4). Given these results, interpretations were largely based on age-detrended data.

3.5. Partition coefficients

Aside from Al, Zn and Pb/Ca, studied molar element/Ca ratios were, on average, lower in the shells than in ultrafiltered seawater (Table 4).

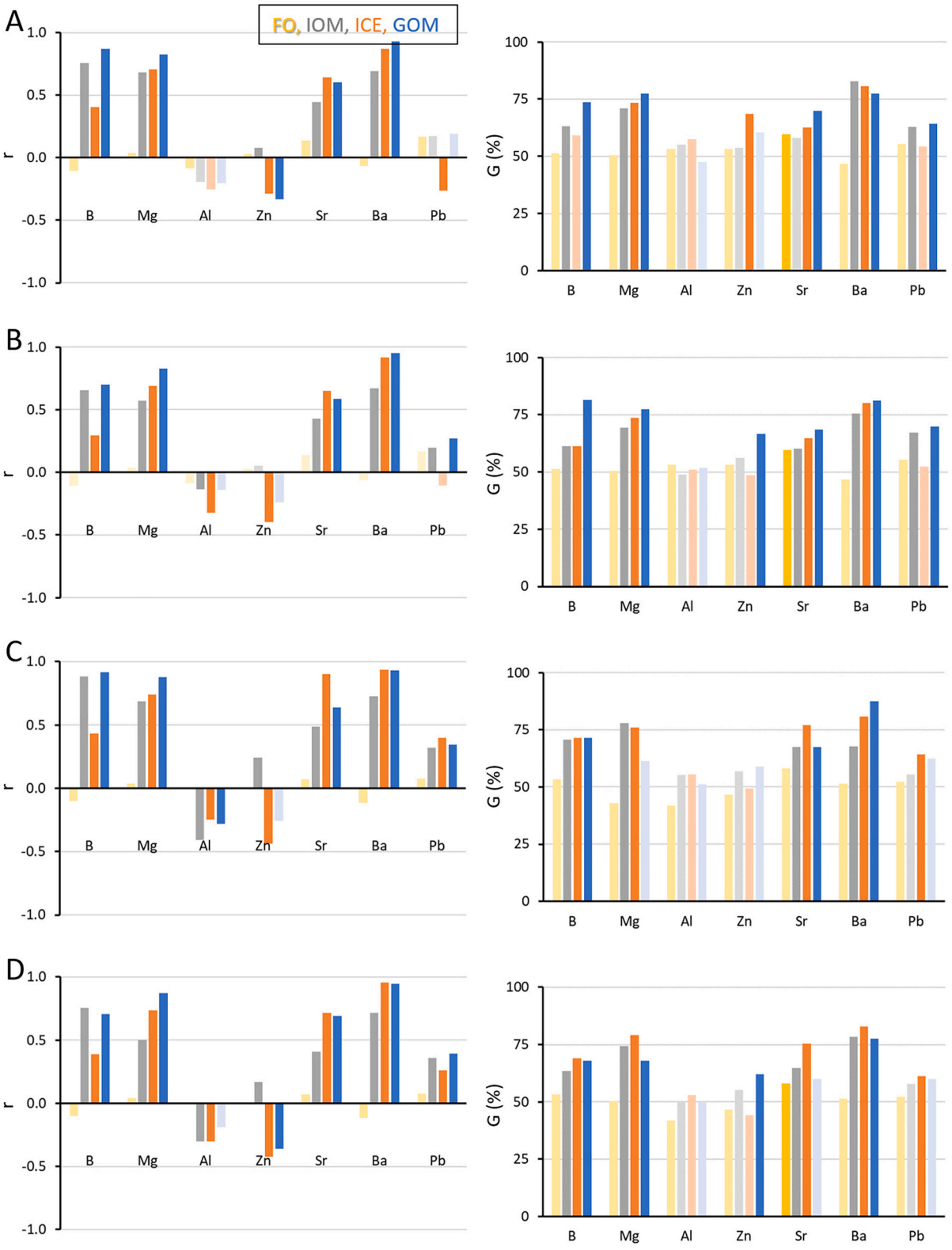

Fig. 2. Agreement between shell element/Ca chronologies (sorted by atomic number) of *Arctica islandica* (hinge portion) evaluated by linear correlation (Pearson r value; left panels) and sign tests (G value = running similarity; right panels). For each locality, the highest r and G values are given. (A) One-by-one comparison, i.e., agreement between two specimens of the same site was assessed. (B) One-versus-others comparison, i.e., agreement between one specimen and the average of all remaining specimens from the same locality was assessed. (C) Same as A, but based on low-pass filtered chronologies. (D) Same as B, but based on low-pass filtered chronologies. FO = Faroe Islands, IOM = Isle of Man, ICE = NE Iceland, GOM = Gulf of Maine. Dark colors indicate significant ($p < 0.05$) agreement, light colors insignificant relationship ($p > 0.05$). Further details are given in Table 2.

Table 2
Agreement between shell element/Ca chronologies (sorted by atomic number) of *Arctica islandica* (hinge portion) evaluated by linear regression analysis (Pearson r value) and sign tests (G value = running similarity). Fig. 2 is the graphic representation of this table. For further explanation see caption of Fig. 2. Red font denotes negative correlation; turquoise font = most values below LOD. Cells highlighted red indicate insignificant r and G values ($p > 0.05$). Blue highlighted cells indicate only correlation is significant, sign-test is not; green stands for the opposite.

Locality↓	B/Ca	Mg/Ca	Al/Ca	Zn/Ca	Sr/Ca	Ba/Ca	Pb/Ca
One-by-one, r values							
FO	-0.10	0.04	-0.09	0.03	0.14	-0.06	0.17
IOM	0.75	0.68	-0.20	0.08	0.44	0.69	0.17
ICE	0.40	0.71	-0.26	-0.29	0.64	0.87	-0.26
GOM	0.87	0.83	-0.20	-0.33	0.60	0.93	0.19
One-by-one, G values							
FO	51.4	50.5	53.2	53.2	59.6	46.8	55.2
IOM	63.2	71.1	55.1	53.7	57.9	82.9	62.8
ICE	59.0	73.2	57.4	68.6	62.7	80.7	54.2
GOM	73.6	77.4	47.6	60.5	69.8	77.4	64.2
One-vs-others, r values							
FO	-0.10	0.04	-0.09	0.03	0.14	-0.06	0.17
IOM	0.66	0.57	-0.14	0.05	0.43	0.67	0.20
ICE	0.29	0.69	-0.32	-0.40	0.65	0.92	-0.11
GOM	0.70	0.83	-0.14	-0.24	0.59	0.95	0.27
One-vs-others, G values							
FO	51.4	50.5	53.2	53.2	59.6	46.8	55.2
IOM	61.3	69.2	48.8	56.1	60.3	75.6	67.1
ICE	61.1	73.6	50.9	48.6	64.7	80.1	52.5
GOM	81.5	77.4	51.9	66.7	68.5	81.1	69.8
Low-pass filtered, one-by-one, r values							
FO	-0.10	0.04	-0.01	0.00	0.07	-0.12	0.07
IOM	0.88	0.69	-0.41	0.24	0.49	0.73	0.32
ICE	0.43	0.74	-0.25	-0.44	0.90	0.94	0.40
GOM	0.92	0.88	-0.28	-0.26	0.64	0.93	0.34
Low-pass filtered, one-by-one, G values							
FO	53.3	42.9	41.9	46.7	58.1	51.4	52.3
IOM	70.6	77.9	55.1	56.8	67.6	67.6	55.4
ICE	71.4	75.9	55.6	49.3	77.2	80.9	64.2
GOM	71.4	61.2	51.3	59.0	67.3	87.5	62.5
Low-pass filtered, one-vs-others, r values							
FO	-0.10	0.04	-0.01	0.00	0.07	-0.12	0.07
IOM	0.76	0.50	-0.30	0.17	0.41	0.72	0.36
ICE	0.39	0.74	-0.30	-0.42	0.72	0.96	0.26
GOM	0.71	0.87	-0.19	-0.36	0.69	0.95	0.39
Low-pass filtered, one-vs-others, G values							
FO	53.3	50.5	41.9	46.7	58.1	51.4	52.3
IOM	63.5	74.3	50.0	55.1	64.9	78.4	57.7
ICE	69.1	79.1	53.1	44.1	75.4	82.8	61.4
GOM	68.0	68.0	50.0	62.0	60.0	77.5	60.0

The strongest depletion (ca. 14,000 times) was observed for magnesium. In contrast, Zn was enriched by nearly four times in the shells, Pb by 71 times, and Al by ca. 94 times. A detailed list of apparent partition coefficients ($K_D^{X/Ca} = \frac{X/Ca_{aragonite}}{X/Ca_{seawater}}$; note $K_D^{B/Ca} = \frac{B/Ca_{aragonite}}{[B(OH)_4^-/HCO_3^-]_{seawater}}$, assuming $[B(OH)_4^-/HCO_3^-_{seawater}] = 0.04$ mol/mol cf. Yu et al., 2007) is listed in Table 4.

Only for six of the studied element/Ca ratios, partition coefficients have been determined in inorganic aragonite (i.e., B, Na, Mg, Zn, Sr, Ba/Ca; Table 4), with sometimes greatly differing results (e.g., B/Ca, Ba/Ca; Table 4). Note, many precipitation experiments were conducted at room temperature. Following these data, Na and Zn/Ca were, on average, 12 and 41% higher in the shells than in inorganic aragonite, whereas the remaining four element/Ca ratios were depleted in *A. islandica* shells by a factor of ca. 3 (Ba/Ca) to 19 (Mg/Ca) (Table 4; Fig. 5; Supplements 5). Depending on the choice of $K_D^{B/Ca}$ value, B/Ca can either be depleted by 12 to 28 times in the shells or enriched by 8 times (Table 4; Fig. 5). Annual Ba, Na and Zn/Ca peaks exceeded respective molar element/Ca values of inorganically precipitated aragonite by up to 13 times (Table 4; Supplements 5).

4. Discussion

4.1. Scope for element-based environmental reconstructions

Based on the findings herein, the question regarding the usability of element chemical data of *A. islandica* as environmental proxies cannot be answered unambiguously. The moderately strong and statistically significant reproducibility between element time-series of contemporaneous specimens after detrending indicates a common response to environmental forcings rather than common physiological trends or spurious agreement (Figs. 2, 4; Table 2). Accordingly, variations in annually-resolved, age- and/or growth rate-detrended time-series of shell B, Mg, Sr and Ba (i.e., elements with concentrations above LOD) were at least partly controlled by external drivers (the same applies to Na, K and Mn/Ca, see Supplements 1 + 3). However, it remains largely unknown which particular environmental variables are encoded in the shells. Actually, the agreement between shell element/Ca ratios and environmental quantities was weaker (up to $R^2 = 0.23$ and G = 66%, site-specific averages of all specimens; Mg/Ca and Sr/Ca vs T and Ba/Ca vs Chl a; IOM, ICE and GOM; low-pass filtered data) than the agreement between respective element/Ca ratios of contemporaneous specimens from the same site (up to $R^2 = 0.44$ and G = 70%, one-versus-others comparison, low-pass filtered data) (Tables 2, 3). This could suggest that the available information on temperature, food, and water chemistry did not properly reflect the environmental conditions which the bivalves experienced or other extrinsic forcings were at work.

A major deficit is also the lack of information on the chemistry of the parent solution from which the shells actually formed, i.e., the extrapallial fluid or gel (EPF). This data would be critically required to compute representative K_D values and calibrate transfer functions. According to the few available studies, the EPF of marine bivalves differs chemically from average seawater (Wada and Fujinuki, 1974, 1976). For example, in the oyster, *Pinctada fucata*, the EPF was enriched in K by 23%, and depleted in Na, Mg, Ca and Sr by 5 to 14% relative to average seawater. Furthermore, the EPF of this species was excessively enriched in redox elements and contained ca. 9100 times more Mn, 23,500 times more Fe, 1250 times more Cu, and 35,400 times more Zn than seawater (Onuma et al., 1979). Note that respective analyses were completed in non-filtered EPF (i.e., the element content of colloids and small particles may have been measured as well). These findings suggest the bivalves inhaled water that differed chemically from average seawater and was very likely influenced by sedimentary porewater (Bruland and Lohan, 2003; Smrzka et al., 2019; Lenstra et al., 2020). Some elements may have also been sourced from digested particles (Martin and Knauer, 1973; Barats et al., 2009, 2010; Thébault et al., 2009, 2022). In addition, the bivalves have presumably actively modified the chemistry of their EPF to facilitate $CaCO_3$ precipitation (e.g., Onuma et al., 1979; Carré et al., 2006). While the data of *P. fucata* are mere snapshots which cannot provide information on how the chemical composition of the EPF changed during the course of time, they clearly illustrate average seawater does not provide a suitable approximation of the EPF chemistry, even in an encrusting, epibenthic bivalve.

Most certainly, the chemical composition of the EPF of *A. islandica* deviated from average seawater as well, which could explain why some of its partition coefficients (shell vs seawater) differed significantly from those computed for inorganic aragonite precipitated from a parent solution resembling seawater chemistry (Table 4; Fig. 5). However, the low K_D values of *A. islandica* (shell vs seawater) for Sr/Ca and Mg/Ca ratios ($K_D^{Sr/Ca} = 0.17$; $K_D^{Mg/Ca} = 0.00007$) can probably not solely be attributed to a different EPF chemistry, because they agree at large with corresponding K_D values of *P. fucata* (shell vs EPF; $K_D^{Sr/Ca} = 0.13$; $K_D^{Mg/Ca} = 0.00016$). Note that the EPF of these bivalves is likely not identical, because *P. fucata* is an epibenthic bivalve, whereas *A. islandica* lives buried in the sediment and is thus more directly exposed to the influence of porewater. Also, both species very likely have different food preferences and thus digest organics with very different chemical composition.

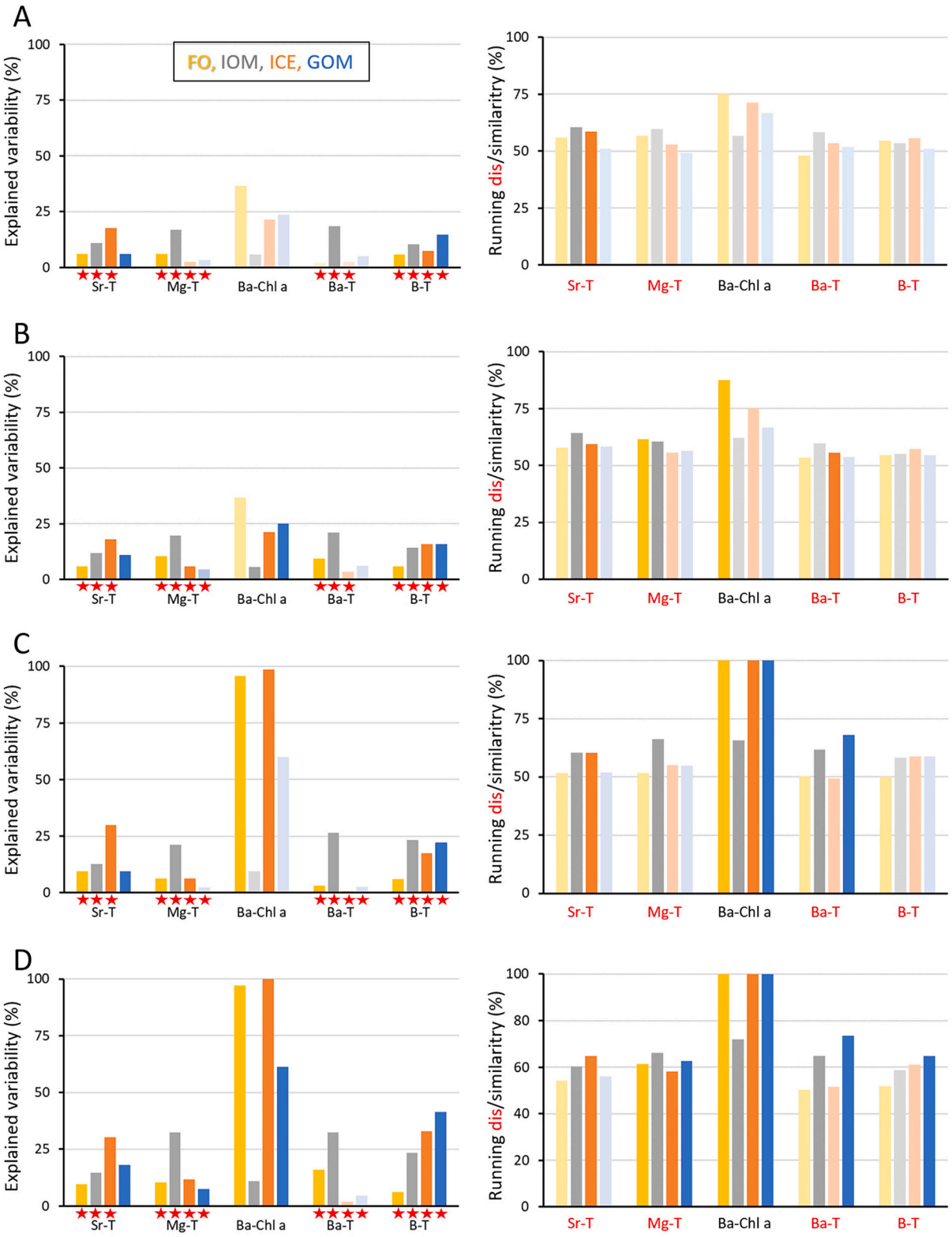

Fig. 3. Agreement between shell element/Ca chronologies (sorted by atomic number) of *Arctica islandica* (hinge portion) and environmental variables. Note, only relationships that were frequently reported in previous studies were investigated. T = water temperature, Chl a = chlorophyll *a*. For each locality, the highest explained variability ($R^2 \times 100$; left panels) and running dis/similarity (right panels) are provided. Red asterisk denotes negative correlation. As expected from inorganic aragonite, the relationship between temperature and Sr, Mg, B or Ba/Ca should be negative and the time-series (T vs element/Ca) run counter to each other; thus, the running dissimilarity was assessed in these cases. (A) Agreement between environmental variable and the site-specific average element/Ca chronology. (B) Agreement between environmental variable and the site-specific element/Ca chronology computed from all but one specimen. (C) Same as A, but based on low-pass filtered chronologies. (D) Same as B, but based on low-pass filtered chronologies. FO = Faroe Islands, IOM = Isle of Man, ICE = NE Iceland, GOM = Gulf of Maine. Dark colors indicate significant ($p < 0.05$) agreement, light colors insignificant relationship ($p > 0.05$). Further details are given in Table 2. (For interpretation of the references to colour in this figure legend, the reader is referred to the web version of this article.)

Table 3
Agreement between shell element/Ca chronologies (sorted by atomic number) of *Arctica islandica* (hinge portion) and environmental variables. For each locality, the highest explained variability ($R^2 \times 100$), highest running similarity (G values) or running dissimilarity (D values, red font) are provided. Fig. 3 is the graphic representation of this table. For further explanation see caption of Fig. 3. Red font in "explained variability" denotes negative correlation. Cells highlighted red indicate insignificant data ($p > 0.05$). Blue highlighted cells indicate that only explained variability is significant, while sign-test is not; green stands for the opposite.

Locality ↓	Sr/Ca-T	Mg/Ca-T	Ba-Chl a	Ba/Ca-T	B/Ca-T
One-by-one, explained variability (%)					
FO	5.9	6.1	36.6	1.8	5.8
IOM	11.0	16.9	5.7	18.4	10.4
ICE	17.5	2.6	21.4	2.4	7.4
GOM	5.9	3.4	23.6	5.0	14.7
One-by-one, G and D values					
FO	55.9	56.6	75.0	48.1	54.4
IOM	60.6	59.7	56.8	58.3	53.5
ICE	58.6	52.9	71.4	53.6	55.7
GOM	50.9	49.1	66.7	51.9	50.9
One-vs-others, explained variability (%)					
FO	5.9	10.4	36.6	9.3	5.8
IOM	11.7	19.5	5.7	21.0	14.1
ICE	18.0	5.9	21.4	3.5	15.9
GOM	10.9	4.6	25.0	6.1	15.8
One-vs-others, G and D values					
FO	57.8	61.5	87.5	53.3	54.4
IOM	64.3	60.6	62.2	59.7	54.9
ICE	59.3	55.7	75.0	55.7	57.1
GOM	58.2	56.4	66.7	53.7	54.5
Low-pass filtered, one-by-one, explained variability (%)					
FO	9.5	6.3	95.7	3.3	6.0
IOM	12.8	21.3	9.6	26.4	23.4
ICE	29.9	6.4	98.6	0.8	32.8
GOM	9.6	2.5	59.9	2.6	21.9
Low-pass filtered, one-by-one, G and D values					
FO	51.5	51.5	100.0	50.4	50.0
IOM	60.3	66.2	65.6	61.8	58.2
ICE	60.3	55.1	100.0	49.3	58.5
GOM	52.0	54.9	100.0	68.0	58.8
Low-pass filtered, one-vs-others, explained variability (%)					
FO	9.5	10.4	97.1	15.9	6.0
IOM	14.7	32.3	10.9	32.4	23.4
ICE	30.4	11.6	100.0	1.9	14.1
GOM	18.1	7.5	61.4	4.6	41.4
Low-pass filtered, one-vs-others, G and D values					
FO	54.3	61.5	100.0	50.4	51.9
IOM	60.3	66.2	71.9	64.7	58.8
ICE	64.7	58.1	100.0	51.5	61.0
GOM	56.0	62.7	100.0	73.5	64.7

As indicated by the K_D values, considerably lower amounts of Sr and Mg ended up in the shells than in inorganic aragonite grown from a parent solution with similar Mg and Sr content as average seawater or EPF of *P. fucata*. Conversely, shells of both bivalve species contained much larger amounts of Sr and Mg as well as other trace and minor impurities than thermodynamically expected or predicted by the lattice strain model (Blundy and Wood, 1994; for calculations see Supplements 5). For example, at the temperatures at which biomineralization occurred, shell Sr/Ca ratios should have varied within a very narrow range around ca. 0.5 mmol/mol (Gaetani and Cohen, 2006) as opposed to the observed 1.34 mmol/mol in *P. fucata* (calculation in Supplements 5) or the annual extremes of 0.78 and 2.92 mmol/mol in *A. islandica* (Table 4). On intra-annual time-scales, shell Sr/Ca of *A. islandica* can fluctuate between values expected for thermodynamic equilibrium within annual increments (fast-growing portion) and at least six to eight times higher values in annual growth lines (= slow-growing portion).

To explain the larger amounts of impurities than expected for a strain-free substitution of Ca^{2+} in the crystal lattice of aragonite by smaller or larger cations, Gaetani and Cohen (2006) evoked the surface entrapment model (Watson, 1996, 2004). Following this hypothesis, rapid precipitation, i.e., fast crystal growth prevents chemical equilibration between the forming solid and the parent solution resulting in the chemical entrapment of the surface region. In addition to or as an alternative to this kinetic process, it is suggested here that the increased ion impurities in the shells result from nonclassical nucleation and growth mechanisms which were observed in many invertebrates (De Yoreo et al., 2015; Boon et al., 2020; Gilbert et al., 2022) including bivalves (Jacob et al., 2011). Thereby, ions such as Mg, Sr and Na that can stabilize amorphous calcium carbonate (ACC) (Schmidt et al., 2019; Boon et al., 2020) – a possible precursor to the formation of $CaCO_3$ (Beniash et al., 1997) – would become incorporated into the forming biomineral. Accordingly, levels of these ions should be higher in fast growing shell portions for which presumably lots of ACC was utilized. However, both models fail to explain the Sr/Ca and Mg/Ca variations in *A. islandica*, because the lowest values were measured in fast-growing shell portions, and vice versa. Thirdly, increased ion impurities in the shells could also result from non-lattice-bound elements, e.g., elements associated with organic matrices (e.g., Onuma et al., 1979; Foster et al., 2008; Takesue et al., 2008; Schöne et al., 2010; Izumida et al., 2011; Yoshimura et al., 2014). While this could contribute to elevated Mg levels near the annual growth lines (Schöne et al., 2010), it cannot explain the high Sr/Ca values in these shell portions. As clearly shown by Foster et al. (2009), Sr^{2+} mainly substitutes for Ca^{2+} in the crystal lattice of aragonite and is barely linked to organics. We speculate here that an unknown physiological process is at work near the biomineralization front that precludes Sr and Mg from incorporation into the shell. When growth slows down and metabolic rates attain a minimum, not enough energy is available to efficiently regulate the incorporation of these ions. Whether the higher than thermodynamically expected levels of other impurities can be explained by one of the three models discussed above, requires more detailed analyses of intra-annual element chemical data in future studies, in particular the concrete relationship with seasonal growth rate variations.

As further shown by Gaetani and Cohen (2006), possibly owing to changes in the "precipitation efficiency", the observed relationship between environmental variables and element/Ca ratios of corals and inorganic aragonite is opposite to thermodynamic predictions and the environmental sensitivity lower than expected (e.g., negative instead of positive correlation between Sr/Ca and T; change of Sr/Ca of −0.04 vs −0.10 mmol/mol per °C). These findings underscore the fact that element-based environmental reconstructions are typically based on empirical relationships rather than theoretical considerations. The observed negative coupling between T and Sr, Mg and B/Ca values in *A. islandica* may thus be likewise valid and useful, at least for qualitative temperature estimates.

While detrended time-series of elements were reproducible between most specimens from the same locality, which was substantiated by statistically significant correlation, running similarity or both, some individuals exhibited only weak or insignificant chemical covariance with other specimens (Fig. 2; Table 2). Potential causes for such reduced reproducibility include differences in microhabitat (changes in benthic fluxes and variable amounts of particles enriched in certain elements) and physiology of the bivalves as well as erroneous temporal alignment. An important conclusion from these observations is that a meaningful interpretation of the shell element chemistry requires data from a sufficiently large number of specimens; comparing merely two shells from the same site is not enough.

In general, our results corroborated the findings by Marali et al. (2017a), although these authors neither adjusted for bias resulting from

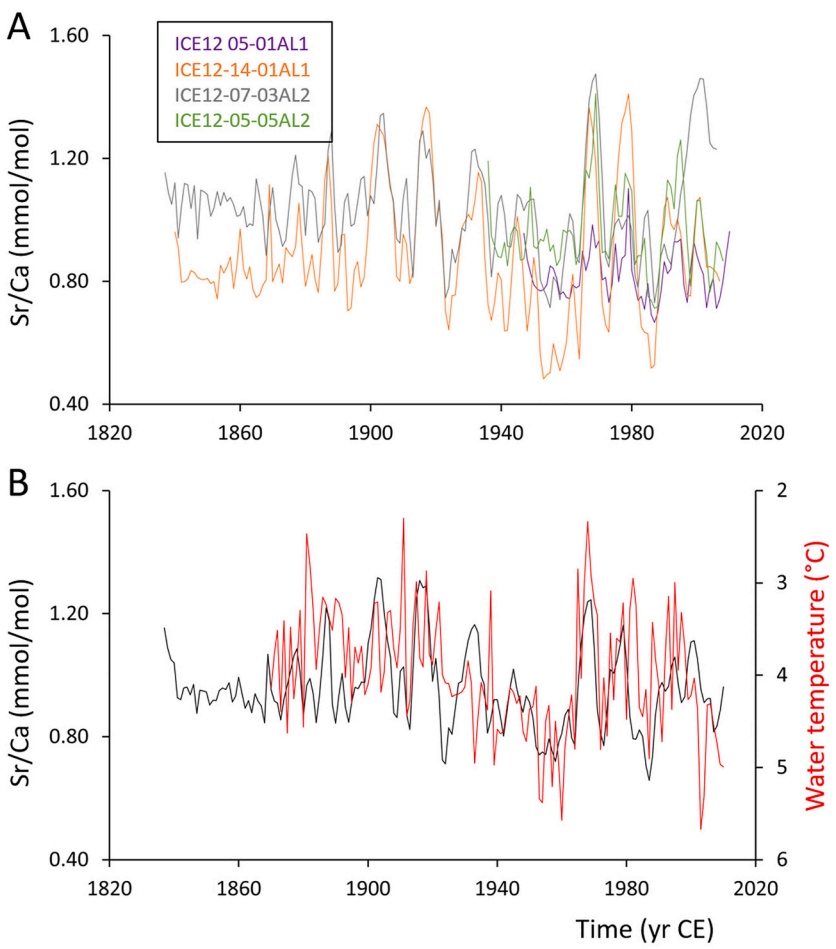

Fig. 4. (A) At NE Iceland, the shell Sr/Ca chronologies of the four specimens of *Arctica islandica* showed notable visual agreement, specifically on quasi-decadal and multidecadal time-scales suggesting that the incorporation of strontium into the shell is partly controlled by an external forcing. (B) The average shell Sr/Ca chronology of that site correlated moderately strongly with instrumental water temperature. After low-pass filtering, 30% of the changes in shell Sr/Ca are mathematically explained by water temperature (see Fig. 3 and Table 3). Note, the temperature axis is inverted. Shell Sr/Ca is anticorrelated to water temperature as the case in inorganic aragonite.

sample geometry, seasonal growth rate variations and ontogenetic age−/growth rate-related trends in element/Ca profiles, nor accounted for possible temporal lags in response to environmental change or minor temporal alignment errors. Though obscured by vital effects, shell element chemical properties of *A. islandica* encode environmental properties, but signal extraction will remain extremely challenging or practically impossible unless much more detailed information is available on the chemistry of the immediate ambient environment, digested food items and the biomineralization fluid including temporal changes thereof. In the following, the potential use of the studied shell element/Ca data as environmental proxies will be discussed in some more detail.

4.1.1. Sr/Ca and Mg/Ca

In agreement with data from inorganic aragonite (Gaetani and Cohen, 2006), Sr and Mg/Ca chronologies of all sites except GOM were significantly negatively correlated with temperature (Fig. 3; Table 3). Up to 30% (ICE) and 32% (IOM) of the variance in age-detrended annual shell Sr/Ca and Mg/Ca values, respectively, were explained by water temperature, which is broadly comparable with previously reported values (41 and 27%, respectively) also determined in the hinge portion of *A. islandica* from Iceland (Schöne et al., 2011). More importantly, detrended Sr/Ca (Fig. 4) and to a lesser degree detrended Mg/Ca curves (Supplements 1) of all four specimens at ICE closely resembled the low-frequency (quasi-decadal, multidecadal) oscillations of water temperature. A similar observation was made by Schöne et al. (2011) in three other shells from the same region. Such a consistent synchrony of element signals cannot be mere chance and this leads to the conclusion that temperature contributes to the variability of annual shell Sr/Ca and Mg/Ca values.

However, opposite results were reported from the relationship between temperature and Sr/Ca or Mg/Ca values of *A. islandica* on intra-annual time-scales, i.e., during the main growing season (= within annual increments). As shown by Wanamaker and Gillikin (2019), in the ventral margin (outer portion of the outer shell layer) of juvenile, laboratory-grown specimens from GOM, Sr/Ca was unrelated and Mg/Ca weakly positively linked to temperature. In field-grown, juvenile ocean quahogs from ICE, Brosset et al. (2022) observed a weak positive correlation between temperature and Sr/Ca values in the (inner portion of the outer shell layer of the) ventral margin, but none in the hinge plate. Notably, mathematical removal of microstructure-related (= biomineral unit area) or growth rate-related effects did not result in any major change of the Sr/Ca vs T relationship (Brosset et al., 2022), suggesting neither growth rate kinetics nor the size of individual biomineral units of the crossed-acicular microstructure had a significant impact on the chemical composition of the shell. However, this does not preclude the possibility that other microstructural variables such as habit of individual biomineral units, crystal surface area etc. or the processes controlling them were important.

Similarly contradictory findings on the relationship between temperature and intra-annual shell Sr or Mg/Ca ratios were reported for many other bivalve species, and even for closely related taxa (Yan et al., 2011, 2013, 2014; Sano et al., 2012). Results reach from negative (Yan et al., 2014; Füllenbach et al., 2015; Zhao et al., 2017a) to positive (Hart and Blusztajn, 1998) to no correlation (Foster et al., 2009; Sano et al., 2012; Poulain et al., 2015; Vihtakari et al., 2016) and encompass field-grown and laboratory-raised specimens (e.g., Yan et al., 2013; Warter et al., 2018). Remarkably, such studies almost always focused on short-lived species or a few selected early ontogenetic years of longer-lived

Table 4
Comparison of the chemical composition of seawater, inorganic aragonite and *Arctica islandica* shells. Seawater chemistry was taken from compilation at MBARI from their website at https://www.mbari.org ("Periodic Table of Elements in the Ocean", lass access: 16 May 2022). Data for the borate/bicarbonate ratio of seawater were taken from Yu et al. (2007). Data of Kinsman (1970) taken from Ram and Erez (2021). Asterisk denotes values calculated for a given temperature using approximation equations provided by cited authors. Av = average; Bgr = background.

Ultrafiltered seawater		Inorganic aragonite			*Arctica islandica*								
X/Ca	Molar ratio	K_D	Ref.	Precipitation conditions	Annual X/Ca					K_D values (2–11 °C)			
					Av	Min	Max	Bgr	Unit	Av	Min	Max	Bgr
B/Ca	40.51 mmol/mol												
$B(OH)_4^-/HCO_3^-$	40 mmol/mol	0.0003–0.03	Mavromatis et al., 2015	T = 5–25 °C, pH = 7.42–9.49	0.10	0.05	0.15		mmol/mol	0.0025	0.0013	0.0038	
		0.071	Holcomb et al., 2016	T = 20–40 °C, pH = 7.4–9.5									
Na/Ca	45.67 mol/mol	0.00040	Kinsman, 1970	T = 15 °C	20.53	16.05	26.96		mmol/mol	0.0004	0.0004	0.0006	
		0.00043	Kitano et al., 1975	T = 25 °C									
Mg/Ca	5.13 mol/mol	0.00047	Gabitov et al., 2011	T = 25 °C	0.38	0.10	0.86		mmol/mol	0.00007	0.00002	0.00017	
		0.00123	AlKhatib and Eisenhauer, 2017	T = 12.5 °C, pH = 8, S = 35.38									
		0.00237	Gaetani and Cohen, 2006	T = 2 °C*									
		0.00189	Gaetani and Cohen, 2006	T = 11 °C*									
		0.00137	Gaetani and Cohen, 2006	T = 25 °C*									
		0.01490	Gaetani and Cohen, 2006	T = 5 °C, pH = 9.65									
		0.00170	Gaetani and Cohen, 2006	T = 15 °C, pH = 9.50									
		0.00133	Gaetani and Cohen, 2006	T = 25 °C, pH = 9.35									
Al/Ca	0.11 µmol/mol				0.01	0.0002	0.20		mmol/mol	92.52	1.85	1850.45	
Mn/Ca	35.05 nmol/mol				3.33	0.37	16.86		µmol/mol	95.00	10.56	480.98	
Zn/Ca	0.53 µmol/mol	3.20	Crocket and Winchester, 1966	T = 50 °C	1.91	0.67	22.03		µmol/mol	3.63	1.27	41.90	
Sr/Ca	8.67 mmol/mol	1.15	DeCarlo et al., 2015	T = 20 °C*, pH = 8.2–8.88	1.50	0.78	2.92		mmol/mol	0.17	0.09	0.34	
		1.17	AlKhatib and Eisenhauer, 2017	T = 12.5 °C, pH = 8, S = 35.38									
		1.27	Dietzel et al., 2004	T = 10 °C									
		1.40	Gaetani and Cohen, 2006	T = 2 °C*									
		1.30	Gaetani and Cohen, 2006	T = 11 °C*									
		1.18	Gaetani and Cohen, 2006	T = 25 °C*									
		0.42	Gaetani and Cohen, 2006	T = 5 °C, pH = 9.65									
		1.24	Gaetani and Cohen, 2006	T = 15 °C, pH = 9.50									
		1.13	Gaetani and Cohen, 2006	T = 25 °C, pH = 9.35									
Ba/Ca	10.61 µmol/mol	0.44	Mavromatis et al., 2018	T = 25 °C, pH = 6.28	5.70	0.76	29.24	2.00	µmol/mol	0.54	0.07	2.75	0.19
		2.07	Dietzel et al., 2004	T = 10 °C									
		6.40	Gaetani and Cohen, 2006	T = 2 °C*									
		4.54	Gaetani and Cohen, 2006	T = 11 °C*									
		2.77	Gaetani and Cohen, 2006	T = 25 °C*									
		1.81	Gaetani and Cohen, 2006	T = 5 °C, pH = 9.65									
		2.99	Gaetani and Cohen, 2006	T = 15 °C, pH = 9.50									
		2.11	Gaetani and Cohen, 2006	T = 25 °C, pH = 9.35									
Pb/Ca	1.27 nmol/mol				0.09	0.03	2.64		µmol/mol	71.10	23.70	2085.60	

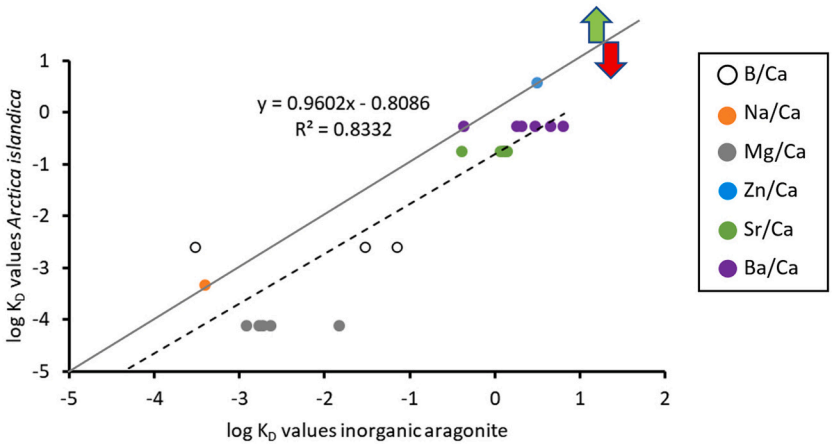

Fig. 5. Partition coefficients of shells of *Arctica islandica* compared to such of inorganic aragonite (references see Table 4). Most element/Ca values are depleted (red arrow) in shells relative to abiogenically precipitated aragonite (values plot below grey curve of unity) suggesting strong vital effects control the incorporation of respective elements into the shell. Na, Ba and Zn are slightly enriched (green arrow) in the shells relative to Ca and plot above the grey curve suggesting that these elements are either biologically enriched in shells or were taken up from other sources. (For interpretation of the references to colour in this figure legend, the reader is referred to the web version of this article.)

species, but rarely included annual Sr/Ca and Mg/Ca time-series covering decades or centuries (Marali et al., 2017a; Schöne et al., 2011). The expected negative coupling between temperature and metal/Ca values only seem to emerge in long element chronologies and when annual resolution is chosen, indicating that the integration of chemical data from annual growth lines could be essential.

In *A. islandica*, intra-annual Sr/Ca and Mg/Ca values of up to ca. 4 and 1 mmol/mol (corresponding to $K_D^{Sr/Ca} = 0.46$ and $K_D^{Mg/Ca} = 0.000195$), respectively, were measured in samples covering annual growth lines (Schöne et al., 2013), but – due to much stronger vital effects and/or different types and amounts if organics – values were three to eight times lower in samples taken within annual increments (Schöne et al., 2011, 2013; Wanamaker and Gillikin, 2019; Brosset et al., 2022). Actual Sr and Mg/Ca ratios at the annual growth lines (few µm broad) are expected to exceed the values listed above, but the sampling resolution (LA spot diameter: 55 µm) was too coarse to determine their precise chemical composition. According to calculations taking the relative proportion within LA spots into account, annual growth lines may contain nearly as much Sr and Mg as observed in abiogenic aragonite indicating that their formation was under reduced vital control (Schöne et al., 2013). This interpretation does not seem unlikely, because during growth line formation, food availability is strongly reduced, the metabolism slow and there was much less energy available to control the element incorporation into the shell (Brosset et al., 2022). Between 2 and 11 °C (the observed annual T range at the four sites of the present study), Sr/Ca and Mg/Ca values of inorganic aragonite would range between 11.28 and 12.11 and 9.72–12.15 mmol/mol, respectively (assuming invariant $Sr/Ca_{water} = 8.67$ mmol/mol and $Mg/Ca_{water} = 5.13$ mol/mol cf. MBARI). These numbers were computed with Eqs. (7) and (8) given by Gaetani and Cohen (2006). If the assumption is correct that vital effects are strongly reduced during annual growth line formation, the Sr/Ca and Mg/Ca values in respective shell portions should register temperature almost as faithfully as inorganic aragonite. The small proportion by which the annual growth lines contribute to the annual metal/Ca averages may explain why the relationship between these elements and temperature is not strong.

Other important issues include the lack of information on the Sr/Ca and Mg/Ca values in the solution from which the shell actually forms as well the sources of these elements in the EPF (i.e., free water column, sedimentary porewater; ions, colloids, particles) and their temporal variability. The successful application of the Sr/Ca or Mg/Ca thermometer critically depends on the chemistry of the biomineralization solution (cf. Vihtakari et al., 2016). While Sr/Ca and Mg/Ca values in the water column above the fluffy layer may be constant within the world ocean on long time-scales (Broecker and Peng, 1982; Nozaki, 1997), they can vary markedly in different portions of the ocean (e.g., in the upper 5 m: $Sr/Ca_{water} = 7.80$ to 10 mmol/mol, $Mg/Ca_{water} = 4.07$ to 6.60 mol/mol, Lebrato et al., 2020) and on short temporal scales (see Supplements 5 for own data from Iceland), e.g., due to riverine influx (de Villiers, 1999). Assuming the same temperature sensitivity as in inorganic aragonite (−0.04 mmol/mol/1 °C; Gaetani and Cohen, 2006), an unnoticed Sr/Ca_{water} change by ±0.15 mmol/mol (which is the approx. Half the range provided by Lebrato et al., 2020, for surface waters of ICE) would translate into a temperature change of ±3.8 °C, which exceeds the inter-annual range at any studied site. Moreover, the chemical composition of the water column does not necessarily reflect that of the water accessed by the bivalves. With its short siphons, *A. islandica* inhales water directly at the sediment water interface (Morton, 2011), i.e., from the fluffy layer, which is influenced by the benthic element fluxes to the ocean (e.g., Bruland and Lohan, 2003). In addition, at least the bivalve foot and parts of the mantle are engulfed by sedimentary porewater, from which ions can reach the body fluids. It should also be kept in mind that the water chemistry is typically determined in filtered (0.22 to 0.45 µm pore diameter; Lu and Wang, 2019) samples and thus reflects a mixture of both the dissolved and small colloid fractions. These two fractions may not necessarily be chemically identical (Martin et al., 2021) nor entirely biologically available for bivalves (Wang and Guo, 2000).

Furthermore, as demonstrated by Ba/Ca (Fig. 1F; and Mn/Ca see Supplements 1), the chemical composition of the body fluids of bivalves is not only determined by the ambient seawater chemistry, but also by elements bound to digested particles (e.g., Sr: Poigner et al., 2012). Therefore, the chemistry of the EPF can differ from that of ultrafiltered seawater. More importantly, aside from seasonally varying dietary composition, the food preferences and food selection capabilities may change during lifetime. In *A. islandica*, diet likely consists of organic detritus during youth, but an increasingly larger proportion of fresh phytoplankton during later stages of life (Schöne et al., 2022). Considering the variable chemical properties of different food items (Martin and Knauer, 1973; Barats et al., 2009, 2010; Thébault et al., 2009; Thébault and Chauvaud, 2013), this can result in significant temporal variability of the chemical composition of the biomineralization solution, which, if it remains unconsidered, can obscure potential temperature signals recorded in shell Sr and Mg/Ca values. Differences in the chemistry of inhaled water and food may also explain the site-specific element/Ca regression curves (especially that at GOM; Fig. 3; Table 2; Supplements 1) and represent the main reason why no universally applicable equation can be provided to compute temperature from shell Sr/Ca or Mg/Ca.

In summary, the strongest argument for a causal link between annual shell Sr/Ca or Mg/Ca data and temperature – besides statistically significant negative correlation and running dissimilarity – is the synchrony of element/Ca profiles and their agreement with low-frequency changes of temperature (Fig. 4). Practically, however, it still remains

impossible to reconstruct quantitative temperature data from annual Sr/Ca and Mg/Ca shell ratios, because only up to about one-third of the chemical variability is explained by temperature and other factors for which no proxies are available (e.g., biomineralization chemistry) obscure the temperature signal. Most importantly, the intercepts of the regression curves differed between sites, which prevents us from establishing a universal metal-based thermometry equation. In order to employ Sr/Ca or Mg/Ca values as paleotemperature proxies, a detailed site-specific calibration would be needed. However, if the transfer function constructed with modern specimens is applied to fossils, the assumption needs to be made that the chemical properties of the biomineralization solution (i.e., the chemistry of inhaled water and food) remained unchanged through time.

4.1.2. Ba/Ca

The strong correlation and synchrony of Ba/Ca series between contemporaneous specimens at IOM, ICE and GOM suggests that Ba incorporation into the shell is driven by a common external forcing, while the lack of reproducibility between the two shells from FO points to significant temporal alignment errors or physiological differences (Fig. 2; Table 2). Ba/Ca profiles of contemporaneous specimens from the same habitat are typically highly synchronous, not only in *A. islandica* (Marali et al., 2017b), but also in many other bivalve species (Barats et al., 2009; Gillikin et al., 2008; Doré et al., 2020). The synchrony is largely driven by sharp erratic Ba/Ca peaks on intra-annual time-scales that typically exceed the low background levels by multiple times (Gillikin et al., 2008; Thébault et al., 2009; Hatch et al., 2013).

Similar to Sr and Mg, the incorporation of Ba is probably biologically controlled, because the background levels (< 2 μmol/mol) remained 24 to 34 times ($K_D^{Ba/Ca} < 0.19$; assuming T = 2–11 °C and invariant Ba/Ca_{water} = 10.61 μmol/mol cf. MBARI) below values observed in abiogenic aragonite (Gaetani and Cohen, 2006: $K_D^{Ba/Ca}$ = 4.54 to 6.40) (Table 4; Fig. 5). Changes of the shell Ba/Ca background reportedly covary with the Ba/Ca_{water} value, which in turn, is inversely coupled to salinity (Gillikin et al., 2005, 2008; Poulain et al., 2015). The sharp erratic peaks (Fig. 1F; best seen in intra-annual chronologies: Supplements 1), however, are most certainly not solely caused by the uptake of barium from the water column, but also by the ingestion and digestion of particulate Ba. This assumption is supported by $K_D^{Ba/Ca}$ values that exceed the corresponding value of inorganic aragonite (Gaetani and Cohen, 2006) by 1.6 to 2.3 times (Table 4). Instead of a strong correlation of shell Ba/Ca peaks with bulk phytoplankton as originally proposed by Stecher III et al. (1996), more recent studies suggest that the ingestion of specific phytoplankton species enriched in barium is responsible for the sharp shell Ba/Ca excursions (Thébault et al., 2009; Fröhlich et al., 2022a). It is therefore not entirely surprising that the correlation and running similarity of shell Ba/Ca with Chl a in the current study often remained below the significance threshold (Fig. 3; Table 3) (and were often weak in previous works, e.g., Gillikin et al., 2008). To identify which particular photoautotrophic species caused the Ba enrichment in the studied shells would require high-resolution chronologies of the abundance and chemical composition of photoautotrophic species that were actually consumed by the ocean quahogs. Such information is currently unavailable for the study sites.

In agreement with observations on synthetically precipitated aragonite, Wanamaker and Gillikin (2019) noticed a negative correlation between intra-annual shell Ba/Ca values of *A. islandica* and ambient water temperature. Evidently, a meaningful link with temperature is only expected in the absence of sharp shell Ba/Ca peaks, which are more strongly controlled by food than salinity or temperature, and unlikely to occur in annually averaged data (Fig. 3; Table 3). To compare annual shell Ba/Ca chronologies with temperature, it would be necessary to cut-out these peaks from the Ba/Ca chronologies. Aside from the fact that this would result in biased annual Ba/Ca averages, an objective separation of background data and peaks appears unfeasible.

4.1.3. B/Ca

A common external driver also seems to have controlled shell B/Ca variations, because at all sites with well-crossdated chronologies, B/Ca series of contemporaneous specimens were significantly correlated with each other and the inter-annual B/Ca variations were significantly synchronized (Figs. 1, 2; Table 2). Chronologies from IOM and GOM covaried particularly strongly with each other. Strong inter-specimen reproducibility was also reported from boron concentrations in shells of other bivalve species (Roopnarine et al., 1998). In planktonic foraminifera (Foster, 2008), scleractinian corals (Allison et al., 2010) and inorganic $CaCO_3$ (Sanyal et al., 2000), B/Ca values are linked to pH, reflecting the relative abundance of borate and boric acid (Hemming and Hanson, 1992; Yu et al., 2007). So far, no strong relationship between pH and B/Ca was verified in bivalves (e.g., McCoy et al., 2011). In the present study, the hypothesis could not be tested, because no suitable instrumental pH chronologies were available for comparison with shell B/Ca values of *A. islandica*. As in *Mytilus californianus* (McCoy et al., 2011), the partitioning of boron between the shell and ambient water was under strong physiological control in *A. islandica*, which is indicated by 12 to 28 times lower B/Ca values than observed in inorganic aragonite (or 8 times higher depending on which K_D values are used) (Table 4; Fig. 5). The low correlation between B/Ca and increment width further suggests that shell growth rate had little to no effect on the incorporation of boron into the shell. Apparently, protons were effectively removed from the biomineralization site (possibly by means of a Na^+/H^+ pump, see Section 4.1.4) – during both slow and fast growth – in order to maintain stable pH conditions at the growth front. It would therefore not be expected that shell B/Ca recorded changes of pH at the site of biomineralization. B/Ca chronologies of the studied ocean quahogs were also not coupled to salinity. Such as link was suggested by Furst et al. (1976) for *M. edulis* and Roopnarine et al. (1998) for *Chione californiensis* and *Chionopsis gnidia*. However, a significant negative correlation (up to 41% explained variability) was detected between shell B/Ca and temperature at all sites (Fig. 3; Table 3), an observation that substantiates previous findings from *Mytilus californianus* shells (McCoy et al., 2011), but differs to observations made for synthetic aragonite (Holcomb et al., 2016), and should thus be investigated in more detail in future studies.

4.1.4. Al/Ca, Zn/Ca, Pb/Ca

Besides episodic peaks, specifically at IOM, the concentrations of these metals largely remained below corresponding detection limits preventing a reliable interpretation of these data (Fig. 1C, D, G). In the following, we will discuss to which extend peaks in shell Al, Zn and Pb/Ca values may have been triggered by environmental forcings.

Lead is toxic to organisms and reaches the ocean in particulate form via rivers or as aerosols that become dissolved in surface waters (Wu and Boyle, 1997; Botté et al., 2022). Dissolved Pb then gets adsorbed to organic particles that sink to the seafloor (Wu and Boyle, 1997) where they can be digested by benthic organisms. Ingestion and digestion of particulate lead may explain the observed Pb/Ca peaks in individual specimens. A small fraction of Pb remains dissolved in the water and is therefore available to bivalves. Lead diffusing out of the sediment (Westerlund et al., 1986) may provide another source for peak Pb/Ca in shells.

As indicated by previous work, bivalve shells can record temporal changes of Pb contamination in the environment (Price and Pearce, 1997; Krause-Nehring et al., 2012; Holland et al., 2014b), but analysis should be based on a large number of specimens to account for large individual differences in Pb/Ca values (Gillikin et al., 2005). In contrast, Vander Putten et al. (2000) suggested that changes in shell Pb/Ca largely mirror seasonally varying amounts of shell organics to which this metal is bound rather than variations of Pb availability in the environment. However, this hypothesis would require that Pb/Ca gradually increases through lifetime paralleling the ontogenetic increase in shell organics, which was not observed in *A. islandica* (Fig. 1G).

Aluminum can impair metabolic functions in invertebrates and is therefore considered a severe toxin (Rosseland et al., 1990). Similar to lead, this pollutant reaches the ocean by atmospheric deposition and riverine influx and binds to particles (Menzel Barraqueta et al., 2020) which can subsequently be consumed by benthic organisms. As aluminum also diffuses out of the sediment (Menzel Barraqueta et al., 2020), bivalves may also assimilate this metal in its dissolved form (Poigner et al., 2012). Like Zn, Al/Ca values were rarely studied at high spatial resolution in marine bivalve shells. Warter et al. (2015) used shell Al/Ca profiles of *Tridacna* along with a range of other element/Ca values as an indicator for diagenesis. Due to the lack of partition coefficients for Al and Pb/Ca of inorganic aragonite, it currently remains difficult to interpret the observed K_D values in the shells (equaling ca. 2 for both metals; Table 4). However, judging from the sharpness of the peaks is appears reasonable to assume that the Al/Ca peaks result from particulate Al uptake or sedimentary porewater efflux.

Free Zn ions are rare in seawater, because this metal forms stable complexes with organic ligands (Bruland, 1989) and is rapidly taken up by phytoplankton (Bruland et al., 1978) for which it serves as the second most essential micronutrient (Rueter and Morel, 1981; Morel et al., 1994; Weber et al., 2018). This likely explains the low Zn/Ca levels (well beyond LOD) in most of the studied shells. In turn, episodic Zn/Ca peaks associated with $K_D^{Zn/Ca}$ values up to 42 times higher than those of inorganic aragonite (Table 4; Fig. 5) point to another source apart from zinc dissolved in seawater. These Zn/Ca peaks potentially reflect large phytoplankton blooms, either caused by the digestion of diatoms or – as suggested by de Winter et al. (2017) – by exposure to increased amounts of Zn^{2+} released at the seafloor during the decay of phytoplankton cells (Bruland et al., 1978; Vance et al., 2017). However, zinc can also reach the oceans in large quantities with urban and industrial wastewater discharges (Wang et al., 2012; Mahboob et al., 2022), causing toxic effects in organisms (Ma et al., 2020) and eventually accumulating in sediments. Digestion of particulate Zn can then become encoded in the shell and interpreted as contamination with this heavy metal. At a dump site of the western Baltic Sea, Liehr et al. (2005), measured average Zn concentrations of ca. 40 ppm in *A. islandica* shells (equivalent to ca. 64 μmol/mol), whereas values at a control site were much lower. For comparison, highest sub-annual peaks at IOM attained 66 μmol/mol (Supplements 1). In connection with the Pb/Ca and Al/Ca peaks (above LOD), strongly elevated Zn/Ca data at IOM (Fig. 1D) more likely result from pollution rather than phytoplankton blooms. As yet, it is unclear at which proportion these metals are incorporated into the shells relative to their concentration in the ambient environment, and therefore no transfer functions are yet available which would be required to quantify the heavy metal pollution. Future calibration work is thus needed.

4.2. Ontogenetic age-related and growth rate-related changes of elements

Due to limited environmental and physiological data as well as missing information on the source and fate of elements, we can only speculate on the possible causes for the observed relationships between element/Ca ratios and ontogenetic age and growth rate (Fig. 1). Ontogenetically increasing amounts of chemical impurities in bivalve shells could have resulted from physiological changes. For example, the ability to preclude certain trace and minor elements from incorporation into the shell may have gradually weakened during lifetime as a result of energy rerouting. To quickly escape the predation window, juvenile bivalves likely devote most energy toward size increase and thus shell formation. Especially, the high demand for Ca^{2+} and HCO_3^- during fast shell growth can only be met by active, i.e., energy-consumptive transport of these ions across the mantle epithelia toward the site of biomineralization (Carré et al., 2006). If the assumption holds true that – due to similar ion radii and charge – active transmembrane transport of Ca^{2+} to the growth front is associated with that of Sr^{2+} (Carré et al., 2006), one would expect increased amounts of strontium to substitute for calcium in the crystal lattice of aragonite in juvenile portions of the shell. However, the opposite was observed herein. Lowest shell Sr/Ca levels were found in the broadest annual increments (Fig. 1E). Furthermore, the incorporation of Sr^{2+} into the shell is unaffected by blocking of Ca^{2+} channels and Ca^{2+}-ATPase in *Corbicula fluminea* suggesting that strontium (as well as Mg and Ba) is not primarily reaching the biomineralization site through such intracellular Ca^{2+} transport mechanisms (Zhao et al., 2017b). In particular during the main growing season (i.e., when the annual increment is formed), Sr^{2+} and other ions were thus most likely actively precluded from the incorporation into the shell. This could have been accomplished, for instance, by specialized transmembrane pumps that transported these ions away from the biomineralization solution or some other, yet unexplained mechanism that caused the lower K_D values than in inorganic aragonite. Such a process would require energy. However, with progressing age, energy is likely increasingly used for gamete production and somatic maintenance instead of rapid biomineralization and removal of unwanted ions. As a consequence, ontogenetically older shell portions contained larger amounts of certain trace impurities (B, Sr, Mg, Al, Zn and Ba; Fig. 1), which can lead to increasingly harder, but also more brittle material (Deng et al., 2022). In addition, slower shell growth was also accompanied by lower amounts of protons generated during $CaCO_3$ formation. Consequently, the activity of ion exchangers, including the Na^+/H^+ pump (Zhao et al., 2017c) decreased, which may explain the exponential decline of shell Na/Ca values during ontogeny (Supplements 1).

Besides active removal of ions from the biomineralization site, the chemistry of the EPF varied in response to ontogenetic changes of food preferences and food selection capabilities (Schöne and Huang, 2021). Following Morton (2011), due to their short siphons, *A. islandica* predominantly consumes suspended organic particles from the fluffy layer as well as organic detritus collected from the sediment floor. Older, larger ocean quahogs, however, can likely produce a stronger inhalant current and thus gain increasing access to fresh phytoplankton in the water body above the fluffy layer. This would fit to the observation by Erlenkeuser (1976) who noted that ocean quahogs are “real gourmets which feed on the most recent organic matter only”. In addition, this is supported by a decline in bulk $\delta^{15}N$ values of shell organic matter (Schöne and Huang, 2021) as well as a gradual decrease in trophic position of the bivalves through ontogeny (Huang et al., 2023). Considering the Ba-enrichment in certain phytoplankton species (Thébault et al., 2009; Fröhlich et al., 2022a), the increasing proportion of fresh phytoplankton in the diet of the bivalves during later stages of life could explain the ontogenetic increase in annual shell Ba/Ca values. At the same time, decreasing amounts of Pb-containing organic particles could have been ingested which resulted in lower Pb/Ca values in shell portions formed later during life (Fig. 1F, G). Along with the ontogenetic shift in diet, the shell protein composition changed (Goodfriend and Weidman, 2001), which may have affected the chemical composition of the shell, because some trace and minor elements are bound to specific organic compounds (e.g., Onuma et al., 1979; Foster et al., 2008; Takesue et al., 2008; Schöne et al., 2010; Izumida et al., 2011; Yoshimura et al., 2014). Future research is certainly needed to shed further light on these issues and clarify which ions other than Sr and Mg can be bound to organic matrices.

With a larger body and the ability to produce a stronger inhalant water current, older bivalves are probably also less strongly influenced by sedimentary porewater efflux, because they can access a larger proportion of water above the fluffy layer. This mechanism has previously been evoked to explain the decreasing shell Mn/Ca values through ontogeny (Schöne et al., 2022) and may likewise apply to other redox-sensitive elements.

While physiological changes can explain the non-linear shifts of many elements through ontogeny, the overall nearly linear increase of shell Sr/Ca and Mg/Ca values (Fig. 1B, E) probably resulted from two antagonizing non-linear trends: a logarithmic increase caused by physiological changes similar to those observed in B/Ca (Fig. 1A) as well as an exponential rise. The latter can be explained by annual averages

computed from an increasingly larger proportion of LA spots covering annual growth lines during lifetime. Considering the significant Sr and Mg enrichment near annual growth lines (Schöne et al., 2013; Shirai et al., 2014) and the exponential decline of shell growth rate, the annual Sr/Ca and Mg/Ca values are expected to increase exponentially through ontogeny and with declining annual increment width. When the logarithmic and exponential curves are combined, the resulting Sr/Ca and Mg/Ca curves show a linear increase.

Despite growth rate being strongly correlated to shell element/Ca values, it still appears unlikely that growth rate-related kinetics exerted a major control on shell element/Ca values. Firstly, non-linear relationships with growth rate were not only observed in Sr/ and Mg/Ca ratios, but also B, Na and Mn/Ca (Fig. 1; Supplements 1). The latter three element/Ca data were not strongly elevated or depleted near annual growth lines and neither did they exhibit any other sharp periodic excursions (Supplements 1). Secondly, after age-detrending, the residuals of all element/Ca values were barely correlated to growth rate any more (Supplements 4). The mathematical elimination of ontogenetic age-related effects from element chronologies removed most of the correlation with increment width. Thirdly, nearly identical Sr/Ca and Mg/Ca values have been measured in contemporaneous shell portions of the hinge and the ventral margin of *A. islandica*, although the former grows considerably slower than the latter (Brosset et al., 2022). The role of precipitation rate (= kinetic) effects on the partition of cations between the calcifying fluid and the mineral has been debated not just in the bivalve sclerochronology community (Dodd, 1965; Stecher III et al., 1996; Takesue and van Geen, 2004; Gillikin et al., 2005; Foster et al., 2009; Schöne et al., 2011; Wanamaker and Gillikin, 2019), but also in studies focusing on inorganically precipitated aragonite. Whereas Sr/Ca ratios increased non-linearly with the rate of inorganic aragonite precipitation in some experiments (Gaetani and Cohen, 2006), no such effect was observed in others (Zhong and Mucci, 1989) demonstrating that environmental parameters were more important.

A more detailed interpretation of the observed relationships between shell element chemistry and ontogenetic age or growth rate would require a thorough analysis of intra-annual data, which is beyond the scope of the present study. In particular, this would allow us to test in detail which elements other than Sr and Mg are empirically linked to the prevailing shell microstructure. Such analyses should be completed in the ventral margin, because this shell portion offers a larger temporal resolution. In addition, LA spot analysis would provide more robust data than the line scan approach, because no data smoothing would occur and the data would be less noisy because measurements are completed on larger amounts of ablated shell material.

4.3. Reproducibility assessment

A meaningful comparison of chronologies requires that each data point represents the same amount of time. Minimizing the time-averaging bias resulting from variations in seasonal shell growth rate is thus a major prerequisite to assess inter-specimen reproducibility and detect potential links between the shell chemistry and environmental variables. For this purpose, weighted annual averages were computed. Without this mathematical transformation, data from fast growing shell portions would have contributed disproportionately strongly to the annual average (Schöne et al., 2022) and masked potentially existing agreement between chronologies.

The agreement between shell chemistry and environmental variables as well as the chemical reproducibility between specimens was subsequently assessed with two different methods, i.e., regression analysis and sign tests. Sign tests are typically used for crossdating (Eckstein and Bauch, 1969), but surprisingly rarely for proxy calibration purposes. Many studied pairs of chronologies yielded statistically significant results for both tests (i.e., positive correlation and running similarity or negative correlation and running dissimilarity) lending strong support to the hypothesis that the chronologies shared common signals. However, in some cases, only one of the two tests returned significant results (Tables 2, 3; Fig. 6A). Statistically significant correlation without significant synchrony can occur if the low-frequency components of two chronologies are synchronized, whereas the high-frequency (year-to-year) changes are not (Fig. 6B). This indicates that the longer-term extrinsic signal is preserved in both series, but individual physiological factors etc. may have controlled element/Ca values on inter-annual time-scales (resulting in low G values). In contrast, two chronologies can exhibit significant running similarity without being significantly correlated to each other (Fig. 6C). In that case, inter-annual environmental variations are driving the synchronization between the chronologies (detectable by sign tests), whereas lower-frequency (physiological and other environmental) components differ between the two chronologies

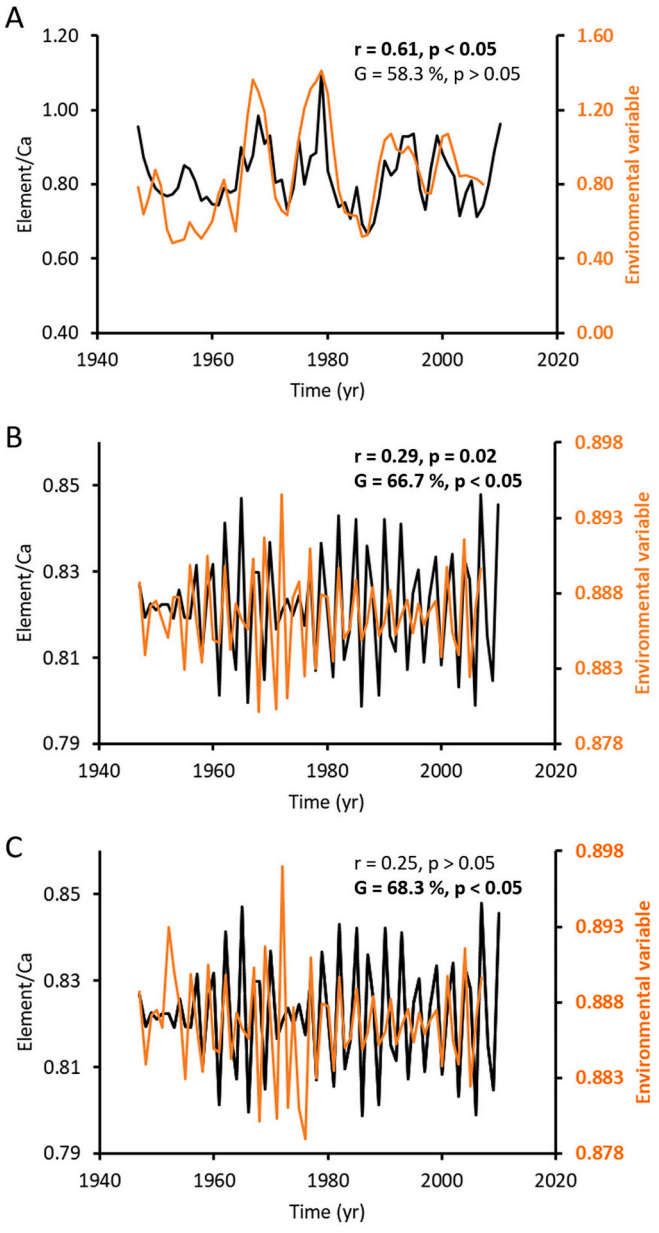

Fig. 6. Numerical models demonstrating how inter-series synchrony can be quantified with regression analysis and sign-tests. (A) Both chronologies are significantly correlated, but year-to-year changes are not statistically significantly similar (running similarity, G values not significant). (B) Both series are significantly correlated with each other and inter-annual changes are synchronous. (C) Correlation remains below significance threshold, but series exhibit significant running similarity.

causing overall weak and insignificant correlation. In both cases where just one test returned significant results, the series preserve common environmental signals and can thus be considered reproducible. By applying sign tests in addition to regression analysis, it was possible to identify reproducibility in incompletely detrended chronologies, i.e., where remaining low-frequency components obscured correlation (Tables 2, 3).

Heteroscedasticity, i.e., the change in data variance through ontogeny is another reason for poor correlation between chronologies including the relatively low correlation between element/Ca chronologies and environmental data sets. Most element time-series showed a gradual weakening of high-frequency oscillations and gradual strengthening of decadal-scale variability through the lifetime of the animal (Fig. 1). Partly, these transient signals may reflect ontogenetic shifts in physiology. Furthermore, elements with strong links to the shell microstructure such as Sr and Mg (both enriched near annual growth lines; Schöne et al., 2013; Shirai et al., 2008), frequency shifts can be explained by an increasing proportion of data from growth lines which contribute to the annual averages as growth rate declines. A similar averaging bias may also occur in element time-series with comparable sharp intra-annual peaks (e.g., B, Na, Al, Ba, and Pb; Supplements 1). Future research is needed to explore possibilities to adjust for such coupled variance differences and produce homoscedastic chronologies.

5. Summary and conclusions

Detrended chronologies of weighted annual B, Mg, Sr and Ba/Ca ratios measured in shells of *A. islandica* were reproducible between most specimens from the same site (Figs. 1, 2; Table 2; the same applies to Na, K and Mn, see Supplements 1 + 3), supporting the hypothesis that the incorporation of these elements is at least partly controlled by environmental forcings. Notably, the element chemical composition of some specimens differed strongly from that of other specimens, which is possibly due to significant physiological differences, microhabitat heterogeneity or poor temporal alignment. It is thus crucial to study a sufficient number of specimens. The coupling between shell element content and environmental variables, was consistently weaker than the inter-specimen reproducibility (Figs. 2, 3; Tables 2, 3), suggesting that in-situ temperature, salinity and oxygen levels which the bivalves actually experienced may have differed from the environmental conditions recorded away from their habitat. Furthermore, the ionic composition of the biomineralization solution from which the shells formed most likely deviated from the average ocean chemistry and also varied through time. If this remains unconsidered, transfer functions will not provide meaningful environmental proxy data. The mixing of chemical data from shell portions consisting of different microstructures or organic materials can further complicate the use of elements as environmental surrogates. However, such links have so far only been studied in a few elements and require future attention.

Unless low-pass filtered, no consistently strong and significant relationship was observed between shell Ba/Ca peaks and Chl a (Fig. 3; Table 3). Judging from findings in other taxa (Thébault et al., 2009; Fröhlich et al., 2022a), sharp Ba/Ca peaks were most likely related to the digestion of specific dinoflagellate and diatom species enriched in barium rather than bulk phytoplankton. If the diet of *A. islandica* was known in detail and temporally highly resolved time-series of the respective food items and their chemical composition were available, it may be possible to properly calibrate the shell Ba/Ca peaks with environmental data and apply this proxy to reconstruct the species composition of past phytoplankton blooms. In conjunction with shell Mo/Ca and Li/Ca data, which are likewise related to specific photoautotrophs (Thébault et al., 2022; Fröhlich et al., 2022b), the species composition may be further constrained and some insight given into relative abundances. It would be required to conduct such calibrations and reconstructions on intra-annual time-scales, because phytoplankton blooms are ephemeral and accordingly, associated Ba/Ca, Mo/Ca and Li/Ca peaks are short-lived (e.g., Gillikin et al., 2008).

The calibration of the Sr, Mg and B/Ca thermometers is significantly more challenging than qualifying the relationship between Ba/Ca and photoautotrophic species, because these elements can be derived from a variety of different sources whose relative proportion varies through time. Temperature could possibly explain a larger proportion of the variance in these element/Ca ratios than that observed in the present study (30 to 40% explained variability; Fig. 3; Table 3) if temporally highly resolved data were available about the (i) chemical composition of the biomineralization solution from which the shell eventually formed and (ii) the actual temperature of the water in which the bivalves lived. The chemistry of the EPF is presumably not only determined by the amounts of dissolved ions in the water above the substrate, but also by the benthic flux of elements into the overlying water body, and the chemical composition of digested food items, colloids and inorganic particles. In other words, the chemical composition of all possible sources of bioavailable elements needs to be determined including their relative contribution to the chemistry of body fluids of bivalves. Controlled tank experiments may provide the best option to investigate these aspects in detail. However, in practice it is probably impossible to reconstruct accurate temperatures from shell Sr, Mg and B/Ca data of (sub)fossil *A. islandica* – and likely most other bivalve species –, because there are no proxies for the EPF chemistry.

Controlled tank studies may also help to further constrain the meaning of coherent variations of other shell element/Ca. For example, pH changes at the growth front of the shells could be monitored and compared to the shell Na/Ca values. Alternatively, the Na^+/H^+ exchanger could be inactivated with specific toxins (similar to the work by Zhao et al., 2017b) in order to test if both pH and shell Na/Ca values decrease. Under laboratory conditions, the concentration of Al, Zn and Pb in the water could also be artificially increased in order to determine the proportion by which these elements are incorporated into the shells. This information is required to quantitatively assess heavy metal pollution with shells of *A. islandica*.

Funding

This study has been made possible by a German Research Foundation (DFG) grant to BRS (SCHO 793/23).

CRediT authorship contribution statement

Bernd R. Schöne: Conceptualization, Data curation, Formal analysis, Investigation, Methodology, Project administration, Supervision, Validation, Visualization, Funding acquisition, Resources, Writing - original draft, Writing - review & editing. **Soraya Marali:** Data curation, Methodology, Formal analysis, Resources, Writing - review & editing. **Anne Jantschke:** Investigation, Writing - review & editing. **Regina Mertz-Kraus:** Resources, Validation, Writing - review & editing. **Paul G. Butler:** Resources, Writing - review & editing. **Lukas Fröhlich:** Formal analysis, Investigation, Methodology, Writing - review & editing.

Declaration of Competing Interest

The authors declare that they have no known competing financial interests or personal relationships that could have appeared to influence the work reported in this paper.

Data availability

Data will be made available on request.

Acknowledgements

We gratefully acknowledge the help of Hilmar A. Holland, Gudrun Thórarinsdóttir, Siggeir Stefánsson, Erlendur Bogason and Sæmundur

Einarsson during fieldwork in Iceland. We thank Una Matras and Ragnar við Streym (SP/F StreymDiving) for making divers available to collect shells near Faroe Islands and Alan D. Wanamaker Jr. for specimens from the Gulf of Maine. Thanks also go to the captain and crew of the RV Prince Madog and of the scalloper Spaven Môr for assistance with the collection of shells from the Isle of Man. We further wish to thank Johanna Boos and Katrin Böhm for their assistance with shell preparation. Comments of two anonymous reviewers helped to improve, streamline and shorten the manuscript; we thank them for their time and suggestions. Furthermore, we thank the DFG for funding this research (grant to BRS, grant# SCHO 793/23).

Appendix A. Supplementary data

Supplementary data to this article can be found online at https://doi.org/10.1016/j.chemgeo.2022.121215.

References

AlKhatib, M., Eisenhauer, A., 2017. Calcium and strontium isotope fractionation during precipitation from aqueous solutions as a function of temperature and reaction rate; II. Aragonite. Geochim. Cosmochim. Acta 209, 320–342. https://doi.org/10.1016/j.gca.2017.04.012.

Allison, N., Finch, A.A., EIMF, 2010. δ^{11}B, Sr, Mg and B in a modern *Porites* coral: the relationship between calcification site pH and skeletal chemistry. Geochim. Cosmochim. Acta 74, 1790–1800. https://doi.org/10.1016/j.gca.2009.12.030.

Barats, A., Amouroux, D., Chauvaud, L., Pécheyran, C., Lorrain, A., Thébault, J., Church, T.M., Donard, O.F.X., 2009. High frequency barium profiles in shells of the Great Scallop *Pecten maximus*: a methodical long-term and multi-site survey in Western Europe. Biogeosciences 6, 157–170. https://doi.org/10.5194/bg-6-157-2009.

Barats, A., Amouroux, D., Pécheyran, C., Chauvaud, L., Thébault, J., Donard, O.F.X., 2010. Spring molybdenum enrichment in scallop shells: a potential tracer of diatom productivity in temperate coastal environments (Brittany, NW France). Biogeosciences 7, 233–245. https://doi.org/10.5194/bg-7-233-2010.

Barker, R.M., 1964. Microtextural variations in pelecypod shells. Malacologia 2, 69–86.

Beniash, E., Aizenberg, J., Addadi, L., Weiner, S., 1997. Amorphous calcium carbonate transforms into calcite during sea urchin larval spicule growth. Proc. R. Soc. Lond. B 264, 461–465. https://doi.org/10.1098/rspb.1997.0066.

Black, B.A., Copenheaver, C.A., Frank, D.C., Stuckey, M.J., Korymanyos, R.E., 2009. Multi-proxy reconstructions of northeastern Pacific sea surface temperature data from trees and Pacific geoduck. Palaeogeogr. Palaeoclimatol. Palaeoecol. 278, 40–47. https://doi.org/10.1016/j.palaeo.2009.04.010.

Blundy, J., Wood, B., 1994. Prediction of crystal-melt partition coefficients from elastic moduli. Nature 372, 452–454. https://doi.org/10.1038/372452a0.

Boon, M., Rickard, W.D.A., Rohl, A.L., Jones, F., 2020. Stabilization of aragonite: role of Mg^{2+} and other impurity ions. Cryst. Growth Des. 20, 5006–5017. https://doi.org/10.1021/acs.cgd.0c00152.

Botté, A., Seguin, C., Nahrgang, J., Zaidi, M., Guery, J., Leignel, V., 2022. Lead in the marine environment: concentrations and effects on invertebrates. Ecotoxicology 31, 194–207. https://doi.org/10.1007/s10646-021-02504-4.

Broecker, W.S., Peng, T.-H., 1982. Tracers in the Sea. Eldigio Press, Palisades, New York, p. 690.

Brosset, C., Höche, N., Shirai, K., Nishida, K., Mertz-Kraus, R., Schöne, B.R., 2022. Strong coupling between biomineral morphology and Sr/Ca of *Arctica islandica* (Bivalvia) — Implications for shell Sr/Ca-based temperature estimates. Minerals 12, 500. https://doi.org/10.3390/min12050500.

Bruland, K.W., 1983. Trace elements in sea-water. In: Riley, J.P., Chester, R. (Eds.), Chemical Oceanography, 8. Academic Press, London, pp. 157–220.

Bruland, K.W., 1989. Complexation of zinc by natural organic ligands in the central North Pacific. Limnol. Oceanogr. 34, 269–285. https://doi.org/10.4319/lo.1989.34.2.0269.

Bruland, K.W., Lohan, M.C., 2003. Controls of trace metals in seawater. In: Treatise on Geochemistry, 6, pp. 23–47. https://doi.org/10.1016/B0-08-043751-6/06105-3.

Bruland, K.W., Knauer, G.A., Martin, J.H., 1978. Zinc in North-East Pacific water. Nature 271, 741–743. https://doi.org/10.1038/271741a0.

Butler, P.G., Richardson, C.A., Scourse, J.D., Wanamaker, A.D., Shammon, T.M., Bennell, J.D., 2010. Marine climate in the Irish Sea: analysis of a 489-year marine master chronology derived from growth increments in the shell of the clam *Arctica islandica*. Quat. Sci. Rev. 29, 1614–1632. https://doi.org/10.1016/j.quascirev.2009.07.010.

Butler, P.G., Wanamaker Jr., A.D., Scourse, J.D., Richardson, C.A., Reynolds, D.J., 2013. Variability of marine climate on the North Icelandic Shelf in a 1357-year proxy archive based on growth increments in the bivalve *Arctica islandica*. Palaeogeogr. Palaeoclimatol. Palaeoecol. 373, 141–151. https://doi.org/10.1016/j.palaeo.2012.01.016.

Byrne, B.H., 2002. Inorganic speciation of dissolved elements in seawater: the influence of pH on concentration ratios. Geochem. Trans. 3, 11–16. https://doi.org/10.1039/b109732f.

Carré, M., Bentaleb, I., Bruguier, O., Ordinola, E., Barrett, N.T., Fontugne, M., 2006. Calcification rate influence on trace element concentrations in aragonitic bivalve shells: evidences and mechanisms. Geochim. Cosmochim. Acta 70, 4906–4920. https://doi.org/10.1016/j.gca.2006.07.019.

Clark II, G.R., 1974. Periodic growth and biological rhythms in experimentally growth bivalves. In: Rosenberg, G.D., Runcorn, S.K. (Eds.), Growth Rhythms and the History of the Earth's Rotation. Wiley, London etc., pp. 103–117

Crocket, J.H., Winchester, J.W., 1966. Coprecipitation of zinc with calcium carbonate. Geochim. Cosmochim. Acta 30, 1093–1109. https://doi.org/10.1016/0016-7037(66)90119-0.

de Villiers, S., 1999. Seawater strontium and Sr/Ca variability in the Atlantic and Pacific. Earth Planet. Sci. Lett. 171, 623–634. https://doi.org/10.1016/S0012-821X(99)00174-0.

de Winter, N.J., Goderis, S., Dehairs, F., Jagt, J.W.M., Fraaije, R.H.B., Van Malderen, S.J.M., Vanhacke, F., Claeys, P., 2017. Tropical seasonality in the late campanian (late cretaceous): comparison between multiproxy records from three bivalve taxa from Oman. Palaeogeogr. Palaeoclimatol. Palaeoecol. 485, 740–760. https://doi.org/10.1016/j.palaeo.2017.07.031.

De Yoreo, J.J., Gilbert, P.U.P.A., Sommerdijk, N.A.J.M., Lee Penn, R., Whitelam, S., Joester, D., Zhang, H., Rimer, J.D., Navrotsky, A., Banfield, J.F., Wallace, A.F., Michel, F.M., Meldrum, F.C., Cölfen, H., Dove, P.M., 2015. Crystallization by particle attachment in synthetic, biogenic, and geologic environments. Science 349. https://doi.org/10.1126/science.aaa6760 aaa6760.

DeCarlo, T.M., Gaetani, G.A., Holcomb, M., Cohen, A.L., 2015. Experimental determination of factors controlling U/Ca of aragonite precipitated from seawater: implications for interpreting coral skeleton. Geochim. Cosmochim. Acta 162, 151–165. https://doi.org/10.1016/j.gca.2015.04.016.

Deng, Z., Jia, Z., Li, L., 2022. Biomineralized materials as model systems for structural composites: intracrystalline structural features and their strengthening and toughening mechanisms. Adv. Sci. 9, 2103524. https://doi.org/10.1002/advs.202103524.

Dietzel, M., Gussone, N., Eisenhauer, A., 2004. Co-precipitation of Sr^{2+} and Ba^{2+} with aragonite by membrane diffusion of CO_2 between 10 and 50°C. Chem. Geol. 203, 139–151. https://doi.org/10.1016/j.chemgeo.2003.09.008.

Dodd, J.R., 1965. Environmental control of strontium and magnesium in *Mytilus*. Geochim. Cosmochim. Acta 29, 385–398. https://doi.org/10.1016/0016-7037(65)90035-9.

Doré, J., Chaillou, G., Poitevin, P., Lazure, P., Poirier, A., Chauvaud, L., Archambault, P., Thébault, J., 2020. Assessment of Ba/Ca in *Arctica islandica* shells as a proxy for phytoplankton dynamics in the Northwestern Atlantic Ocean. Estuar. Coast. Shelf Sci. 237, 106628 https://doi.org/10.1016/j.ecss.2020.106628.

Eckstein, D., Bauch, J., 1969. Beitrag zur Rationalisierung eines dendrochronologischen Verfahrens und zur Analyse seiner Aussagesicherheit. Forstwissensch. Centralbl. 88, 230–250. https://doi.org/10.1007/bf02741777.

Edge, D.C., Reynolds, D.J., Wanamaker, A.D., Griffin, D., Bureau, D., Outridge, C., Stevick, B.C., Weng, R., Black, B.A., 2021. A multicentennial proxy record of Northeast Pacific sea surface temperatures from the annual growth increments of *Panopea generosa*. Paleoceanogr. Paleoclimatol. 36 https://doi.org/10.1029/2021PA004291 e2021PA004291.

Erlenkeuser, H., 1976. ^{14}C and ^{13}C isotope concentration in modem marine mussels from sedimentary habitats. Naturwissenschaften 63, 338. https://doi.org/10.1007/bf00597312.

Evans, J.W., 1972. Tidal growth increments in the cockle *Clinocardium nuttalli*. Science 176, 416–417. https://doi.org/10.1126/science.176.4033.416.

Foster, G.L., 2008. Seawater pH, pCO_2 and $[CO_3^{2-}]$ variations in the Caribbean Sea over the last 130 kyr: a boron isotope and B/Ca study of planktic foraminifera. Earth Planet. Sci. Lett. 271, 254–266. https://doi.org/10.1016/j.epsl.2008.04.015.

Foster, L.C., Finch, A.A., Allison, N., Andersson, C., Clarke, L.J., 2008. Mg in aragonite bivalve shells: seasonal variations and mode of incorporation in *Arctica islandica*. Chem. Geol. 254, 113–119. https://doi.org/10.1016/j.chemgeo.2008.06.007.

Foster, L.C., Allison, N., Finch, A.A., Andersson, C., 2009. Strontium distribution in the shell of the aragonite bivalve *Arctica islandica*. Geochem. Geophys. Geosyst. 10 https://doi.org/10.1029/2007gc001915. Q03003.

Fox, M., Tripathy-Lang, A., Shuster, D.L., 2017. Improved spatial resolution of elemental maps through inversion of LA-ICPMS data. Chem. Geol. 467, 30–41. https://doi.org/10.1016/j.chemgeo.2017.07.001.

Fritz, L.W., Ragone, L.M., Lutz, R.A., 1990. Biomineralization of barite in the shell of the freshwater Asiatic clam *Corbicula fluminea* (Mollusca: Bivalvia). Limnol. Oceanogr. 35, 756–763. https://doi.org/10.4319/lo.1990.35.3.0756.

Fröhlich, L., Siebert, V., Walliser, E.O., Thébault, J., Jochum, K.P., Chauvaud, L., Schöne, B.R., 2022a. Ba/Ca profiles in shells of *Pecten maximus* – a proxy for specific primary producers rather than bulk phytoplankton. Chem. Geol. 593, 120743 https://doi.org/10.1016/j.chemgeo.2022.120743.

Fröhlich, L., Siebert, V., Huang, Q., Thébault, J., Jochum, K.P., Schöne, B.R., 2022b. Deciphering the potential of Ba/Ca, Mo/Ca and Li/Ca profiles in the bivalve shell *Pecten maximus* as proxies for the reconstruction of phytoplankton dynamics. Ecol. Indic. 141, 109121 https://doi.org/10.1016/j.ecolind.2022.109121.

Füllenbach, C.S., Schöne, B.R., Mertz-Kraus, R., 2015. Strontium/lithium ratio in shells of *Cerastoderma edule* (Bivalvia) – a new potential temperature proxy for brackish environments. Chem. Geol. 417, 341–355. https://doi.org/10.1016/j.chemgeo.2015.10.030.

Furst, M., Lowenstam, H.A., Burnett, D.S., 1976. Radiographic study of the distribution of boron in recent mollusc shells. Geochim. Cosmochim. Acta 40, 1381–1386. https://doi.org/10.1016/0016-7037(76)90128-9.

Gabitov, R.I., Schmitt, A.K., Rosner, M., McKeegan, K.D., Gaetani, G.A., Cohen, A.L., Watson, E.B., Harrison, T.M., 2011. In situ δ^7Li, Li/Ca, and Mg/Ca analyses of

synthetic aragonites. Geochem. Geophys. Geosyst. 12, Q03001. https://doi.org/10.1029/2010GC003322.
Gaetani, G.A., Cohen, A.L., 2006. Element partitioning during precipitation of aragonite from seawater: a framework for understanding paleoproxies. Geochim. Cosmochim. Acta 70, 4617–4634. https://doi.org/10.1016/j.gca.2006.07.008.
Gilbert, P.U.P.A., Bergmann, K.D., Boekelheide, N., Tambutte, S., Mass, T., Marin, F., Adkins, J.F., Erez, J., Gilbert, B., Knutson, V., Cantine, M., Hernández, J.O., Knoll, A. H., 2022. Biomineralization: integrating mechanism and evolutionary history. Sci. Adv. 8 https://doi.org/10.1126/sciadv.abl9653 eabl9653.
Gillikin, D.P., Dehairs, F., Baeyens, W., Navez, J., Lorrain, A., André, L., 2005. Inter- and intra-annual variations of Pb/Ca ratios in clam shells (*Mercenaria mercenaria*): a record of anthropogenic lead pollution? Mar. Pollut. Bull. 50, 1530–1540. https://doi.org/10.1016/j.marpolbul.2005.06.020.
Gillikin, D.P., Lorrain, A., Paulet, Y.M., André, L., Dehairs, F., 2008. Synchronous barium peaks in high-resolution profiles of calcite and aragonite marine bivalve shells. Geo-Mar. Lett. 28, 351–358. https://doi.org/10.1007/s00367-008-0111-9.
Goodfriend, G.A., Weidman, C.R., 2001. Ontogenetic trends in aspartic acid racemization and amino acid composition within modern and fossil shells of the bivalve Arctica. Geochim. Cosmochim. Acta 65, 1921–1932. https://doi.org/10.1016/S0016-7037(01)00564-6.
Griffin, S.M., 2012. Applying Dendrochronology Visual Crossdating Techniques to the Marine Bivalve *Arctica islandica* and Assessing the Utility of Master Growth Chronologies as Proxies for Temperature and Secondary Productivity in the Gulf of Maine. Unpublished Master's Thesis. Iowa State University, Ames, IA, p. 237. https://doi.org/10.31274/etd-180810-1103.
Hart, S.R., Blusztajn, J., 1998. Clams as recorders of ocean ridge volcanism and hydrothermal vent field activity. Science 280, 883–886. https://doi.org/10.1126/science.280.5365.883.
Hatch, M.B.A., Schellenberg, S.A., Carter, M.L., 2013. Ba/Ca variations in the modern intertidal bean clam *Donax gouldii*: an upwelling proxy? Palaeogeogr. Palaeoclimatol. Palaeoecol. 373, 98–107. https://doi.org/10.1016/j.palaeo.2012.03.006.
Hemming, N.G., Hanson, G.N., 1992. Boron isotopic composition and concentration in modern marine carbonates. Geochim. Cosmochim. Acta 56, 537–543, 1992. https://doi.org/10.1016/0016-7037(92)90151-8.
Höche, N., Walliser, E.O., Schöne, B.R., 2022. Microstructural mapping of *Arctica islandica* shells reveals environmental and physiological controls on biomineral size. Front. Earth Sci. 781305 https://doi.org/10.3389/feart.2021.781305.
Holcomb, M., DeCarlo, T.M., Gaetani, G.A., McCulloch, M., 2016. Factors affecting B/Ca ratios in synthetic aragonite. Chem. Geol. 437, 67–76. https://doi.org/10.1016/j.chemgeo.2016.05.007.
Holland, H.A., Schöne, B.R., Lipowski, C., Esper, J., 2014a. Decadal climate variability of the North Sea during the last millennium reconstructed from bivalve shells (*Arctica islandica*). The Holocene 24, 771–786. https://doi.org/10.1177/0959683614530438.
Holland, H.A., Schöne, B.R., Marali, S., Jochum, K.P., 2014b. History of bioavailable lead and iron in the Greater North Sea and Iceland during the last millennium – a bivalve sclerochronological reconstruction. Mar. Pollut. Bull. 87, 104–116. https://doi.org/10.1016/j.marpolbul.2014.08.005.
Holmes, R.L., 1983. Computer-assisted quality control in tree-ring dating and measurement. Tree-Ring Bull. 43, 69–78.
Huang, Q., Wu, H., Schöne, B.R., 2023. A novel trophic archive: Practical considerations of compound-specific amino acid $\delta^{15}N$ analysis of carbonate-bound organic matter in bivalve shells (*Arctica islandica*). Chem. Geol. 615, 121220 https://doi.org/10.1016/j.chemgeo.2022.121220.
Izumida, H., Yoshimura, T., Suzuki, A., Nakashima, R., Ishimura, T., Yasuhara, M., Inamura, A., Shikazono, N., Kawahata, H., 2011. Biological and water chemistry controls on Sr/Ca, Ba/Ca, Mg/Ca and $\delta^{18}O$ profiles in freshwater pearl mussel *Hyriopsis* sp. Palaeogeogr. Palaeoclimatol. Palaeoecol. 309, 298–308. https://doi.org/10.1016/j.palaeo.2011.06.014.
Jacob, D.E., Wirth, R., Soldati, A.L., Wehrmeister, U., Schreiber, A., 2011. Amorphous calcium carbonate in the shells of adult Unionoida. J. Struct. Biol. 173, 241–249. https://doi.org/10.1016/j.jsb.2010.09.011.
Jochum, K.P., Nohl, U., Herwig, K., Lammel, E., Stoll, B., Hofmann, A.W., 2005. GeoReM: a new geochemical database for reference materials and isotopic standards. Geostand. Geoanal. Res. 29, 333–338. https://doi.org/10.1111/j.1751–908X.2005.tb00904.x.
Jochum, K.P., Weis, U., Stoll, B., Kuzmin, D., Yang, Q., Raczek, I., Jacob, D.E., Stracke, A., Birbaum, K., Frick, D.A., Günther, D., Enzweiler, J., 2011. Determination of reference values for NIST SRM 610–617 glasses following ISO guidelines. Geostand. Geoanal. Res. 35, 397–429. https://doi.org/10.1111/j.1751–908X.2011.00120.x.
Jochum, K.P., Scholz, D., Stoll, B., Weis, U., Wilson, S.A., Yang, Q., Schwalb, A., Börner, N., Jacob, D.E., Andreae, M.O., 2012. Accurate trace element analysis of speleothems and biogenic calcium carbonates by LA-ICP-MS. Chem. Geol. 318–319, 31–44. https://doi.org/10.1016/j.chemgeo.2012.05.009.
Jones, D.S., 1980. Annual cycle of shell growth increment formation in two continental shelf bivalves and its paleoecologic significance. Paleobiology 6, 331–340. https://doi.org/10.1017/S0094837300006837.
Jones, D.S., Arthur, M.A., Allard, D.J., 1989. Sclerochronological records of temperature and growth from shells of *Mercenaria mercenaria* from Narragansett Bay, Rhode Island. Mar. Biol. 102, 225–234. https://doi.org/10.1007/bf00428284.
Kitano, Y., Okumura, M., Idogaki, M., 1975. Incorporation of sodium, chloride and sulfate with calcium carbonate. Geochem. J. 9, 75–84. https://doi.org/10.2343/geochemj.9.75.
Komagoe, T., Watanabe, T., Shirai, K., Yamazaki, A., Uematu, M., 2018. Geochemical and microstructural signals in giant clam *Tridacna maxima* recorded typhoon events at Okinotori Island, Japan. J. Geophys. Res. Biogeosci. 123, 1460–1474. https://doi.org/10.1029/2017jg004082.
Krause-Nehring, J., Brey, T., Thorrold, S.R., 2012. Centennial records of lead contamination in northern Atlantic bivalves (*Arctica islandica*). Mar. Pollut. Bull. 64, 233–240. https://doi.org/10.1016/j.marpolbul.2011.11.028.
Lazareth, C.E., Vander Putten, E., André, L., Dehairs, F., 2003. High-resolution trace element profiles in shells of the mangrove bivalve *Isognomon ephippium*: a record of environmental spatio-temporal variations? Estuar. Coast. Shelf Sci. 57, 1103–1114. https://doi.org/10.1016/S0272-7714(03)00013-1.
Lebrato, M., Garbe-Schönberg, D., Müller, M.N., Blanco-Ameijeiras, S., Feely, R.A., Lorenzoni, L., Molinero, J.-C., Bremer, K., Jones, D.O.B., Iglesias-Rodriguez, D., Greeley, D., Lamare, M.D., Paulmier, A., Graco, M., Cartes, J., Barcelos e Ramos, J., de Lara, A., Sanchez-Leal, R., Jimenez, P., Paparazzo, F.E., Hartman, S.E., Westernströer, U., Küter, M., Benavides, R., da Silva, A.F., Bell, S., Payne, C., Olafsdottir, S., Robinson, K., Jantunen, L.M., Korablev, A., Webster, R.J., Jones, E. M., Gilg, O., Bailly du Bois, P., Beldowski, J., Ashjian, C., Yahia, N.D., Twining, B., Chen, X.-G., Tseng, L.-C., Hwang, J.-S., Dahms, H.-U., Oschlies, A., 2020. Global variability in seawater Mg:Ca and Sr:Ca ratios in the modern ocean. Proc. Natl. Acad. Sci. U. S. A. 117, 22281–22292. https://doi.org/10.1073/pnas.1918943117.
Lenstra, W.K., Hermans, M., Séguret, M.J.M., Witbaard, R., Severmann, S., Behrends, T., Slomp, C.P., 2020. Coastal hypoxia and eutrophication as key controls on benthic release and water column dynamics of iron and manganese. Limnol. Oceanogr. 66, 807–826. https://doi.org/10.1002/lno.11644.
Liehr, G.A., Zettler, M.L., Leipe, T., Witt, G., 2005. The ocean quahog *Arctica islandica* L.: a bioindicator for contaminated sediments. Mar. Biol. 147, 671–679. https://doi.org/10.1007/s00227-005-1612-y.
Lohmann, G., Schöne, B.R., 2013. Climate signatures on decadal to interdecadal time scales as obtained from mollusk shells (*Arctica islandica*) from Iceland. Palaeogeogr. Palaeoclimatol. Palaeoecol. 373, 152–162. https://doi.org/10.1016/j.palaeo.2012.08.006.
Lu, G.-Y., Wang, W.-X., 2019. Water analysis | seawater: inorganic compounds for environmental analysis. In: Encyclopedia of Analytical Science, Third ed., pp. 353–358. https://doi.org/10.1016/B978-0-12-409547-2.14498-1.
Ma, J., Wang, W., Liu, X., Wang, Z., Gao, G., Wu, H., Li, X., Xu, J., 2020. Zinc toxicity alters the photosynthetic response of red alga *Pyropia yezoensis* to ocean acidification. Environ. Sci. Pollut. Res. 27, 3202–3212. https://doi.org/10.1007/s11356-019-06872-7.
Mahboob, S., Ahmed, Z., Khan, M.F., Virik, P., Al-Mulhm, N., Baabbad, A.A.A., 2022. Assessment of heavy metals pollution in seawater and sediments in the Arabian Gulf, near Dammam, Saudi Arabia. J. King Saud Univ. Sci. 34, 101677 https://doi.org/10.1016/j.jksus.2021.101677.
Marali, S., Schöne, B.R., Mertz-Kraus, R., Griffin, S.M., Wanamaker Jr., A.D., Butler, P.G., Holland, H.A., Jochum, K.P., 2017a. Reproducibility of trace element variations (Na/Ca, Mg/Ca, Mn/Ca, Sr/Ca, and Ba/Ca) within and between specimens of the bivalve *Arctica islandica* – a LA-ICP-MS line scan study. Palaeogeogr. Palaeoclimatol. Palaeoecol. 484, 109–128. https://doi.org/10.1016/j.palaeo.2016.11.024.
Marali, S., Schöne, B.R., Mertz-Kraus, R., Griffin, S.M., Wanamaker Jr., A.D., Matras, U., Butler, P.G., 2017b. Ba/Ca ratios in shells of *Arctica islandica* – potential environmental proxy and crossdating tool. Palaeogeogr. Palaeoclimatol. Palaeoecol. 465, 347–361. https://doi.org/10.1016/j.palaeo.2015.12.018.
Marchitto Jr., T.M., Jones, G.A., Goodfriend, G.A., Weidman, C.R., 2000. Precise temporal correlation of Holocene mollusk shells using sclerochronology. Quat. Res. 53, 236–246. https://doi.org/10.1006/qres.1999.2107.
Martin, J.H., Knauer, G.A., 1973. The elemental composition of plankton. Geochim. Cosmochim. Acta 37, 1639–1658. https://doi.org/10.1016/0016-7037(73)90154-3.
Martin, L.A., Vignati, D.A.L., Hissler, C., 2021. Contrasting distribution of REE and yttrium among particulate, colloidal and dissolved fractions during low and high flows in peri-urban and agricultural river systems. Sci. Total Environ. 790, 148207 https://doi.org/10.1016/j.scitotenv.2021.148207.
Mavromatis, V., Montouillout, V., Noireaux, J., Gaillardet, J., Schott, J., 2015. Characterization of boron incorporation and speciation in calcite and aragonite from co-precipitation experiments under controlled pH, temperature and precipitation rate. Geochim. Cosmochim. Acta 150, 299–313. https://doi.org/10.1016/j.gca.2018.06.018.
Mavromatis, V., Goetschl, K.E., Grengg, C., Konrad, F., Purgstaller, B., Dietzel, M., 2018. Barium partitioning in calcite and aragonite as a function of growth rate. Geochim. Cosmochim. Acta 237, 65–78. https://doi.org/10.1016/j.gca.2014.10.024.
McCoy, S.J., Robinson, L.F., Pfister, C.A., Wootton, J.T., Shimizu, N., 2011. Exploring B/Ca as a pH proxy in bivalves: relationships between *Mytilus californianus* B/Ca and environmental data from the Northeast Pacific. Biogeosciences 8, 2567–2579. https://doi.org/10.5194/bg-8-2567-2011.
Menzel Barraqueta, J.-L., Samanta, S., Achterberg, E.P., Bowie, A.R., Croot, P., Cloete, R., De Jongh, T., Gelado-Caballero, M.D., Klar, J.K., Middag, R., Loock, J.C., Remenyi, T.A., Wenzel, B., Roychoudhury, A.N., 2020. A first global oceanic compilation of observational dissolved aluminum data with regional statistical data treatment. Front. Mar. Sci. 7, 468. https://doi.org/10.3389/fmars.2020.00468.
Morel, F.M.M., Reinfelder, J.R., Roberts, S.B., Chamberlain, C.P., Lee, J.G., Yee, D., 1994. Zinc and carbon co-limitation of marine phytoplankton. Nature 369, 740–742. https://doi.org/10.1038/369740a0.
Morton, B., 2011. The biology and functional morphology of *Arctica islandica* (Bivalvia: Arcticidae): a gerontophilic living fossil. Mar. Biol. Res. 7, 540–553. https://doi.org/10.1080/17451000.2010.535833.
Nozaki, Y., 1997. A fresh look at element distribution in the North Pacific. EOS 78, 221.

Onuma, N., Masuda, F., Masataka, H., Wada, K., 1979. Crystal structure control on trace element partition in molluscan shell formation. Geochem. J. 13, 187–189. https://doi.org/10.2343/geochemj.13.187.

Peharda, M., Schöne, B.R., Black, B.A., Corrège, T., 2021. Advances of sclerochronology research in the last decade. Palaeogeogr. Palaeoclimatol. Palaeoecol. 570, 110371 https://doi.org/10.1016/j.palaeo.2021.110371.

Poigner, H., Monien, D., Monien, P., Kriews, M., Brumsack, H.-J., Wilhelms-Dick, D., Abele, D., 2012. Element ratios between digestive gland and gill tissues of the Antarctic bivalve *Laternula elliptica* as a proxy for element uptake from different environmental sources. Geophys. Res. Abstr. 14. EGU2012-6576.

Poulain, C., Gillikin, D.P., Thébault, J., Munaron, J.M., Bohn, M., Robertm, R., Paulet, Y.-M., Lorrain, A., 2015. An evaluation of Mg/Ca, Sr/Ca, and Ba/Ca ratios as environmental proxies in aragonite bivalve shells. Chem. Geol. 396, 42–50. https://doi.org/10.1016/j.chemgeo.2014.12.019.

Price, G.D., Pearce, N.J.G., 1997. Biomonitoring of pollution by *Cerastoderma edule* from the British Isles: a Laser Ablation ICP-MS study. Mar. Pollut. Bull. 34, 1025–1031. https://doi.org/10.1016/S0025-326X(97)00098-2.

Ram, S., Erez, J., 2021. The distribution coefficients of major and minor elements in coral skeletons under variable calcium seawater concentration. Front. Earth Sci. 9, 657176 https://doi.org/10.3389/feart.2021.657176.

Reynolds, D.J., Scourse, J.D., Halloran, P.R., Nederbragt, A.J., Wanamaker, A.D., Butler, P.G., Richardson, C.A., Heinemeier, J., Eiríksson, J., Knudsen, K.L., Hall, I.R., 2016. Annually resolved North Atlantic marine climate over the last millennium. Nat. Commun. 7, 13502. https://doi.org/10.1038/ncomms13502.

Reynolds, D.J., Hall, I.R., Slater, S.M., Scourse, J.D., Halloran, P.R., Sayer, M.D.J., 2017. Reconstructing past seasonal to multicentennial-scale variability in the NE Atlantic Ocean using the long-lived marine bivalve mollusk *Glycymeris glycymeris*. Palaeoceanography 32, 1153–1173. https://doi.org/10.1002/2017pa003154.

Roesijadi, G., 1992. Metallothioneins in metal regulation and toxicity in aquatic animals. Aquat. Toxicol. 22, 81–114. https://doi.org/10.1016/0166-445X(92)90026-J.

Roger, L.M., George, A.D., Shaw, J., Hart, R.D., Roberts, M., Becker, R., McDonald, B.J., Evans, N.J., 2017. Geochemical and microstructural characterisation of two species of cool-water bivalves (*Fulvia tenuicostata* and *Soletellina biradiata*) from Western Australia. Biogeosciences 14, 1721–1737. https://doi.org/10.5194/bg-14-1721-2017.

Roopnarine, P.D., Fitzgerald, P., Byars, G., Kilb, K., 1998. Coincident boron profiles of bivalves from the Gulf of California: implications for the calculation of paleosalinities. Palaios 13, 395–400. https://doi.org/10.2307/3515327.

Rosseland, B.O., Eldhuset, T.D., Staurnes, M., 1990. Environmental effects of aluminium. Environ. Geochem. Health 12, 17–27. https://doi.org/10.1007/bf01734045.

Rueter, J.G., Morel, F.M.M., 1981. The interaction between zinc deficiency and copper toxicity as it affects the silicic acid uptake mechanisms in *Thalassiosira pseudonana*. Limnol. Oceanogr. 26, 67–73. https://doi.org/10.4319/lo.1981.26.1.0067.

Sano, Y., Kobayashi, S., Shirai, K., Takahata, N., Matsumoto, K., Watanabe, T., Sowa, K., Iwai, K., 2012. Past daily light cycle recorded in the strontium/calcium ratios of giant clam shells. Nat. Commun. 3, 761. https://doi.org/10.1038/ncomms1763.

Sanyal, A., Nugent, M., Reeder, R.J., Bijma, J., 2000. Seawater pH control on the boron isotopic composition of calcite: evidence from inorganic calcite precipitation experiments. Geochim. Cosmochim. Acta 64, 1551–1555.

Schmidt, I., Zolotoyabko, E., Lee, K., Gjardy, A., Berner, A., Lakin, E., Fratzl, P., Wagermaier, W., 2019. Effect of strontium ions on crystallization of amorphous calcium carbonate. Cryst. Growth Des. 54 https://doi.org/10.1002/crat.201900002, 1900002.

Schöne, B.R., Huang, Q., 2021. Ontogenetic $\delta^{15}N$ trends and multidecadal variability in shells of the bivalve mollusk, *Arctica islandica*. Front. Mar. Sci. 8, 748593 https://doi.org/10.3389/fmars.2021.748593.

Schöne, B.R., Krause, R.A., 2016. Retrospective environmental biomonitoring – Mussel watch expanded. Glob. Planet. Chang. 144, 228–251. https://doi.org/10.1016/j.gloplacha.2016.08.002.

Schöne, B.R., Oschmann, W., Kröncke, I., Dreyer, W., Janssen, R., Rumohr, H., Houk, S. D., Freyre Castro, A.D., Dunca, E., Rössler, J., 2003. North Atlantic Oscillation dynamics recorded in shells of a long-lived bivalve mollusk. Geology 31, 1037–1040. https://doi.org/10.1130/G20013.1.

Schöne, B.R., Fiebig, J., Pfeiffer, M., Gleß, R., Hickson, J., Johnson, A.L.A., Dreyer, W., Oschmann, W., 2005. Climate records from a bivalved Methuselah (*Arctica islandica*, Mollusca; Iceland). Palaeogeogr. Palaeoclimatol. Palaeoecol. 228, 130–148. https://doi.org/10.1016/j.palaeo.2005.03.049.

Schöne, B.R., Zhang, Z., Jacob, D., Gillikin, D.P., Tütken, T., Garbe-Schönberg, D., McConnaughey, T., Soldati, A., 2010. Effect of organic matrices on the determination of the trace element chemistry (Mg, Sr, Mg/Ca, Sr/Ca) of aragonitic bivalve shells (*Arctica islandica*) – comparison of ICP-OES and LA-ICP-MS data. Geochem. J. 44, 23–37. https://doi.org/10.2343/geochemj.1.0045.

Schöne, B.R., Zhang, Z., Radermacher, P., Thébault, J., Jacob, D., Nunn, E.V., Maurer, A. F., 2011. Sr/Ca and Mg/Ca ratios of ontogenetically old, long-lived bivalve shells (*Arctica islandica*) and their function as paleotemperature proxies. Palaeogeogr. Palaeoclimatol. Palaeoecol. 286, 52–64. https://doi.org/10.1016/j.palaeo.2010.03.016.

Schöne, B.R., Radermacher, P., Zhang, Z., Jacob, D.E., 2013. Crystal fabrics and element impurities (Sr/Ca, Mg/Ca, and Ba/Ca) in shells of *Arctica islandica* – Implications for paleoclimate reconstructions. Palaeogeogr. Palaeoclimatol. Palaeoecol. 373, 50–59. https://doi.org/10.1016/j.palaeo.2011.05.013.

Schöne, B.R., Marali, S., Mertz-Kraus, R., Butler, P.G., Wanamaker Jr., A.D., Fröhlich, L., 2022. Importance of weighting high-resolution proxy data from bivalve shells to avoid bias caused by sample spot geometry and variability in seasonal growth rate. Front. Earth Sci. 10, 889115 https://doi.org/10.3389/feart.2022.889115.

Shirai, K., Schöne, B.R., Miyaji, T., Radermacher, P., Krause Jr., R.A., Tanabe, K., 2014. Assessment of the mechanism of elemental incorporation into bivalve shells (*Arctica islandica*) based on elemental distribution at the ultrastructural scale. Geochim. Cosmochim. Acta 126, 307–320. https://doi.org/10.1016/j.gca.2013.10.050.

Shirai, K., Takahata, N., Yamamoto, H., Omata, T., Sasaki, T., Sano, Y., 2008. Novel analytical approach to bivalve shell biogeochemistry: A case study of hydrothermal mussel shell. Geochem. J. 42, 413–420. https://doi.org/10.2343/geochemj.42.413.

Smrzka, D., Zwicker, J., Bach, W., Feng, D., Himmler, T., Chen, D., Peckmann, J., 2019. The behavior of trace elements in seawater, sedimentary pore water, and their incorporation into carbonate minerals: a review. Facies 65, 41. https://doi.org/10.1007/s10347-019-0581-4.

Stecher III, H.A., Krantz, D.E., Lord III, C.J., Luther III, G.W., Bock, K.W., 1996. Profiles of strontium and barium in *Mercenaria mercenaria* and *Spisula solidissima* shells. Geochim. Cosmochim. Acta 60, 3445–3456. https://doi.org/10.1016/0016-7037(96)00179-2.

Takesue, R.K., van Geen, A., 2004. Mg/Ca, Sr/Ca, and stable isotopes in modern and Holocene *Protothaca staminea* shells from a northern California coastal upwelling region. Geochim. Cosmochim. Acta 68, 3845–3861. https://doi.org/10.1016/j.gca.2004.03.021.

Takesue, R.K., Bacon, C.R., Thompson, J.K., 2008. Influences of organic matter and calcification rate on trace elements in aragonitic estuarine bivalve shells. Geochim. Cosmochim. Acta 72, 5431–5445. https://doi.org/10.1016/j.gca.2008.09.003.

Thébault, J., Chauvaud, L., 2013. Li/Ca enrichments in great scallop shells (*Pecten maximus*) and their relationship with phytoplankton blooms. Palaeogeogr. Palaeoclimatol. Palaeoecol. 373, 108–122. https://doi.org/10.1016/j.palaeo.2011.12.014.

Thébault, J., Chauvaud, L., L'Helguen, S., Clavier, J., Barats, A., Jacquet, S., Pécheyran, C., Amouroux, D., 2009. Barium and molybdenum records in bivalve shells: geochemical proxies for phytoplankton dynamics in coastal environments? Limnol. Oceanogr. 54, 1002–1014. https://doi.org/10.4319/lo.2009.54.3.1002.

Thébault, J., Jolivet, A., Waeles, M., Tabouret, H., Saboret, S., Pécheyran, P., Leynaert, A., Jochum, K.P., Schöne, B.R., Fröhlich, L., Siebert, V., Amice, E., Chauvaud, L., 2022. Scallop shells as geochemical archives of phytoplankton-related ecological processes in a temperate coastal ecosystem. Limnol. Oceanogr. 67, 187–202. https://doi.org/10.1002/lno.11985.

Thomson, J.D., Pirie, B.J.S., George, S.G., 1985. Cellular metal distribution in the pacific oyster, *Crassostrea gigas* (Thun.) determined by quantitative X-ray microprobe analysis. J. Exp. Mar. Biol. Ecol. 85, 37–45. https://doi.org/10.1016/0022-0981(85)90012-7.

Vance, D., Little, S., de Souza, G.F., Shatiwala, S.P., Lohan, M.C., Middag, R., 2017. Silicon and zinc biogeochemical cycles coupled through the Southern Ocean. Nat. Geosci. 10, 202–206. https://doi.org/10.1038/ngeo2890.

Vander Putten, E., Dehairs, F., Keppens, E., Baeyens, W., 2000. High resolution distribution of trace elements in the calcite shell layer of modern *Mytilus edulis*: environmental and biological controls. Geochim. Cosmochim. Acta 64, 997–1011. https://doi.org/10.1016/S0016-7037(99)00380-4.

Viarengo, A., 1989. Heavy metals in marine invertebrates: mechanisms of regulation and toxicity at the cellular level. Rev. Aquat. Sci. 1, 295–317.

Vihtakari, M., Ambrose Jr., W.G., Renaud, P.E., Locke, V.W.L., Carroll, M.L., Berge, J., Clarke, L.J., Cottier, F., Hop, H., 2016. A key to the past? Element ratios as environmental proxies in two Arctic bivalves. Palaeogeogr. Palaeoclimatol. Palaeoecol. 465, 316–332. https://doi.org/10.1016/j.palaeo.2016.10.020.

Wada, K., Fujinuki, T., 1974. Physiological regulation of shell formation in molluscs. I. Chemical composition of extrapallial fluid. Bull. Natl. Pearl Res. Lab. 18, 2085–2110.

Wada, K., Fujinuki, T., 1976. Biomineralization in bivalve molluscs with emphasis on the chemical composition of the extrapallial fluid. In: Watabe, N., Wilbur, K.M. (Eds.), The Mechanism of Mineralization in the Invertebrates and Plants. Belle W. Baruch Library in Marine Science Series, 5. University of South Carolina Press, pp. 175–190.

Wanamaker, A.D., Gillikin, D.P., 2019. Strontium, magnesium, and barium incorporation in aragonitic shells of juvenile *Arctica islandica*: insights from temperature controlled experiments. Chem. Geol. 526, 117–129. https://doi.org/10.1016/j.chemgeo.2018.02.012.

Wanamaker Jr., A.D., Heinemeier, J., Scourse, J.D., Richardson, C.A., Butler, P.G., Eiríksson, J., Knudsen, K.L., 2008. Very long-lived mollusks confirm 17th century AD tephra-based radiocarbon reservoir ages for North Icelandic shelf waters. Radiocarbon 50, 399–412. https://doi.org/10.1017/S0033822200053510.

Wanamaker Jr., A.D., Butler, P.G., Scourse, J.D., Heinemeier, J., Eiríksson, J., Knudsen, K.L., Richardson, C.A., 2012. Surface changes in the North Atlantic meridional overturning circulation during the last millennium. Nat. Commun. 3, 899. https://doi.org/10.1038/ncomms1901.

Wanamaker Jr., A.D., Griffin, S.M., Ummenhofer, C.C., Whitney, N.M., Black, B., Parfitt, R., Lower-Spies, E.E., Introne, D., Kreutz, K.J., 2019. Pacific climate influences on ocean conditions and extreme shell growth events in the Northwestern Atlantic (Gulf of Maine). Clim. Dyn. 52, 6339–6356. https://doi.org/10.1007/s00382-018-4513-8.

Wang, W.-X., Guo, L., 2000. Influences of natural colloids on metal bioavailability to two marine bivalves. Environ. Sci. Technol. 34, 4571–4576. https://doi.org/10.1021/es000933v.

Wang, J., Liu, R.H., Yu, P., Tang, A.K., Xu, L.Q., Wang, J.Y., 2012. Study on the pollution characteristics of heavy metals in seawater of Jinzhou Bay. Procedia Environ. Sci. 13, 1507–1516. https://doi.org/10.1016/j.proenv.2012.01.143.

Warter, V., Erez, J., Müller, W., 2018. Environmental and physiological controls on daily trace element incorporation in *Tridacna crocea* from combined laboratory culturing and ultra-high resolution LA-ICP-MS analysis. Palaeogeogr. Palaeoclimatol. Palaeoecol. 496, 32–47. https://doi.org/10.1016/j.palaeo.2017.12.038.

Warter, V., Müller, W., Wesselingh, F.P., Todd, J.A., Renema, W., 2015. Late Miocene seasonal to subdecadal climate variability in the Indo-West Pacific (East Kalimantan, Indonesia) preserved in giant clams. Palaios 30, 66–82. https://doi.org/10.2110/palo.2013.061.

Watson, E.B., 1996. Surface enrichment and trace-element uptake during crystal growth. Geochim. Cosmochim. Acta 60, 5013–5020. https://doi.org/10.1016/S0016-7037(96)00299-2.

Watson, E.B., 2004. A conceptual model for near-surface kinetic controls on the trace-element and stable isotope composition of abiogenic calcite crystals. Geochim. Cosmochim. Acta 68, 1473–1488. https://doi.org/10.1016/j.gca.2003.10.003.

Weber, T., John, S., Tagliabue, A., DeVries, T., 2018. Biological uptake and reversible scavenging of zinc in the global ocean. Science 361, 72–76. https://doi.org/10.1126/science.aap8532.

Weidman, C.R., Jones, G.A., Lohmann, K.C., 1994. The long-lived mollusc *Arctica islandica*: a new paleoceanographic tool for the reconstruction of bottom temperatures for the continental shelves of the northern North Atlantic Ocean. J. Geophys. Res. 99, 18305–18314. https://doi.org/10.1029/94jc01882.

Westerlund, S.F.G., Anderson, L.G., Hall, P.O.J., Iverfeldt, Å., Rutgers van der Loeff, M. M., Sundby, B., 1986. Benthic fluxes of cadmium, copper, nickel, zinc and lead in the coastal environment. Geochim. Cosmochim. Acta 50, 1289–1296. https://doi.org/10.1016/0016-7037(86)90412-6.

Witbaard, R., Duineveld, G.C.A., deWilde, P.A.W.J., 1997. A long-term growth record derived from *Arctica islandica* (Mollusca, Bivalvia) from the Fladen Ground (northern North Sea). J. Mar. Biol. Assoc. U. K. 77, 801–816. https://doi.org/10.1017/S0025315400036201.

Wu, J., Boyle, E.A., 1997. Lead in the western North Atlantic Ocean: completed response to leaded gasoline phaseout. Geochim. Cosmochim. Acta 61, 3279–3283. https://doi.org/10.1016/S0016-7037(97)89711-6.

Yan, H., Shao, D., Wang, Y.-H., Sun, L.-G., 2011. High resolution Sr/Ca profile of Tridacna gigas from Xisha Islands of South China Sea and its potential application on sea surface temperature reconstruction. J. Earth Environ. 2, 381–386.

Yan, H., Shao, D., Wang, Y., Sun, L., 2013. Sr/Ca profile of long-lived *Tridacna gigas* bivalves from South China Sea: a new high-resolution SST proxy. Geochim. Cosmochim. Acta 112, 52–65. https://doi.org/10.1016/j.gca.2013.03.007.

Yan, H., Shao, D., Wang, Y., Sun, L., 2014. Sr/Ca differences within and among three Tridacnidae species from the South China Sea: implication for paleoclimate reconstruction. Chem. Geol. 390, 22–31. https://doi.org/10.1016/j.chemgeo.2014.10.011.

Yoshimura, T., Tamenori, Y., Kawahata, H., Suzuki, A., 2014. Fluctuations of sulfate, S-bearing amino acids and magnesium in a giant clam shell. Biogeosciences 11, 3881–3886. https://doi.org/10.5194/bg-11-3881-2014.

Yu, J., Elderfield, H., Hönisch, B., 2007. Tropical sea-surface temperature reconstruction for the early Paleogene using Mg/Ca ratios of planktonic foraminifera. Paleoceanography 22. https://doi.org/10.1029/2006PA001347. PA2202.

Zhao, L., Schöne, B.R., Mertz-Kraus, R., 2017a. Controls on strontium and barium incorporation into freshwater bivalve shells (*Corbicula fluminea*). Palaeogeogr. Palaeoclimatol. Palaeoecol. 465, 386–394. https://doi.org/10.1016/j.palaeo.2015.11.040.

Zhao, L., Schöne, B.R., Mertz-Kraus, R., 2017b. Delineating the role of calcium in shell formation and elemental composition of *Corbicula fluminea* (Bivalvia). Hydrobiologia 790, 259–272. https://doi.org/10.1007/s10750-016-3037-7.

Zhao, L., Schöne, B.R., Mertz-Kraus, R., Yang, F., 2017c. Insights from sodium into the impacts of elevated pCO_2 and temperature on bivalve shell formation. J. Exp. Mar. Biol. Ecol. 486, 148–154. https://doi.org/10.1016/j.jembe.2016.10.009.

Zhong, S., Mucci, A., 1989. Calcite and aragonite precipitation from seawater solutions of various salinities: precipitation rates and overgrowth compositions. Chem. Geol. 78, 283–299. https://doi.org/10.1016/0009-2541(89)90064-8.